Stockholm University

Bachelor Thesis

Degree Project in Geology 15 hp

A sedimentological study of Cryogenian glacial-interglacial cycles recorded by the Port Askaig Tillite Formation on Islay, Scotland

Martin Dahlgren

Stockholm 2018

Department of Geological Sciences
Stockholm University
SE-106 91 Stockholm
Sweden

Abstract

An interglacial mudstone sequence from the Port Askaig Tillite Formation on Islay was analysed using an Olympus XRF detector. The resulting geochemical log was compared with an XRF dataset acquired from a Quaternary sedimentary core from the Lomonosov Ridge in the Arctic Ocean. Chemical proxies representing climatic and environmental changes were analysed in an effort to specifically identify evidence of orbital forcing in the Cryogenian Period.

The studied non-glacial rock-section from the Port Askaig Formation was interpreted as being deposited in a shallow marine setting at semitropical latitudes during an episode of global warming at some stage of the Sturtian glaciation (ca 717 – 660 Ma). The transport mechanism of glaciogenic material was by ice rafting. High hematite content was interpreted as an oxygenation event in a peritidal zone when isostatic rebound caused a sea level regression. Increasing amount of muscovite is interpreted to indicate increased weathering. Underlaying sequence of dolostone and overlaying sequence of sandstone were consistent with these interpretations. One interglacial phase is thus observed, which possibly could be attributed to Milankovitch orbital forcing.

The interpretation of the paleoclimatic setting of the studied interglacial mudstone did not provide support for the Snowball Earth hypothesis in its “hard” version. Neither did other observations such as evidence of repeating glacial-interglacial cycles and banded iron formations (BIF) appearing also within the Sturtian glaciation.

Table of contents

1 Introduction and geological framework…… 3
1.1 Introduction…… 3
1.2 The Cryogenian Period and the Snowball Earth hypothesis…… 4
1.2.1 The Cryogenian Period…… 4
1.2.2 Observations leading up to the Snowball Earth hypothesis…… 5
1.2.3 The Snowball Earth hypothesis…… 6
1.2.4 Alternative explanations…… 8
1.3 The Port Askaig Tillite Formation…… 9
1.3.1 Short geological history of Islay and overall stratigraphy…… 9
1.3.2 Port Askaig Formation – age and paleogeography…… 11
1.3.3 Port Askaig Formation – stratigraphy…… 12
1.3.4 Tectonic setting for the build-up of the Port Askaig Formation. 13
1.3.5 Possible depositional mechanisms and paleoenvironment…… 13
1.4 The Arctic Ocean during the Quaternary and its sedimentation environment. 14
1.4.1 The Quaternary Period…… 14
1.4.2 The Arctic Ocean…… 16
1.4.3 Transport mechanisms and sedimentary regimes of glaciogenic materials…… 17
1.4.4 Milankovitch orbital forcing of climate change…… 18
1.5 Review of proxies for climatic and environmental change…… 19
2 Methodology…… 21
2.1 The analyse method…… 21
2.2 Description of field measurements of interglacial sequence done on Islay…… 23
2.3 Description of lab measurements on Arctic Ocean sediment core…… 24
2.4 Data handling…… 25
3 Results…… 26
3.1 Reliability of data…… 26
3.2 Internal correlation between elements in each dataset…… 27
3.3 Port Askaig interglacial mudstone data…… 28
3.4 AO96/12-1pc data…… 31
4 Discussion…… 36
4.1 Interpretation of proxy data and discussion about possible orbital driven cycles…… 36
4.2 A paleoclimatic and paleoenvironmental interpretation of the Port Askaig interglacial section …… 37
4.3 Interpretation of other observations…… 41
5 Conclusions…… 42
6 Acknowledgements…… 43
7 References…… 43

1. Introduction and geological framework

1.1 Introduction

The Cryogenian Period was a dramatic time with extreme climate shifts and two lengthy periods when the Earth was almost fully covered by ice. The hydrological cycle stopped, life almost collapsed, and the oceans became anoxic (Hoffman et al, 1998; Hoffman et al, 2017). The return to warmth was as dramatic with extreme CO_2 levels in the atmosphere, rapidly melting ices and raising sea levels (Hoffman et al, 1998; Hoffman et al, 2017). A model has been proposed to provide possible explanations for what happened and its causes – the Snowball Earth hypothesis (Hoffman et al, 1998). There are however observations which do not correspond with predictions generated by this hypothesis (Fairchild and Kennedy, 2007), and the subject is intensely debated.

There are some analogies that can be made between the drama of the Cryogenian and our present days. In a geological time-frame, Earth also now goes through a dramatic change. We are not able to predict the full extent of the climate changes we will experience in the coming 100 years. There are feedback mechanisms which are still unclear to us with possibilities of nonlinear responses and Earth shifting into a full greenhouse state (IPCC, 2014).

A better understanding of the Cryogenian and the Snowball Earth hypothesis as an analogy for tipping points where positive feedbacks take over, may help us to better predict what will happen to the Earth we live on today.

Much work has been done concerning these topics. Research about our Pliocene – Pleistocene glacial-interglacial history which very much is linked to the Arctic region, and ongoing efforts to build evidence for or against or refining the Snowball Earth hypothesis, are just two of many active areas of study. This bachelor thesis will in some limited way address these two areas. The aim of this bachelor thesis project is to study glacial-interglacial cycles recorded by the Port Askaig Tillite Formation on Islay, Scotland. The Port Askaig Tillite Formation consists of 47 glaciogenic diamictite horizons which are interlayered with non-glacial rocks. This study focuses on the non-glacial mudstone sequence in between the diamictite horizon no 13 and 14.

The aim is to construct sedimentary and geochemical logs of this non-glacial sequence and compare this log with a Pleistocene–Holocene sequence from an Arctic Ocean sediment core. The study will focus on certain proxies linked to glacial-interglacial variability of e.g. chemical weathering, river denudation and oxygenation that can survive greenschist facies metamorphism. This study will also document evidence (if any) of orbital forcing in the Cryogenian Period, perhaps in the final stages of a Snowball Earth glaciation.

The goals of this project are:

- To construct a cm-scale sedimentary and geochemical log of one sequence of non-glacial rocks separating glaciogenic diamictites in the Port Askaig Tillite Formation on Islay, Scotland. This is done using an Olympus portable XRF analyser capable of determining elemental concentration in the field.
- To compare this log with the results of previous proxy studies linked to glacial-interglacial variations and to a chemical log from a sediment core from the Lomonosov Ridge in the Arctic Ocean, produced using the same portable XRF analyser.
- To write and motivate a paleoclimatic/environmental interpretation for the section of non-glacial rocks from the Port Askaig Tillite Formation.

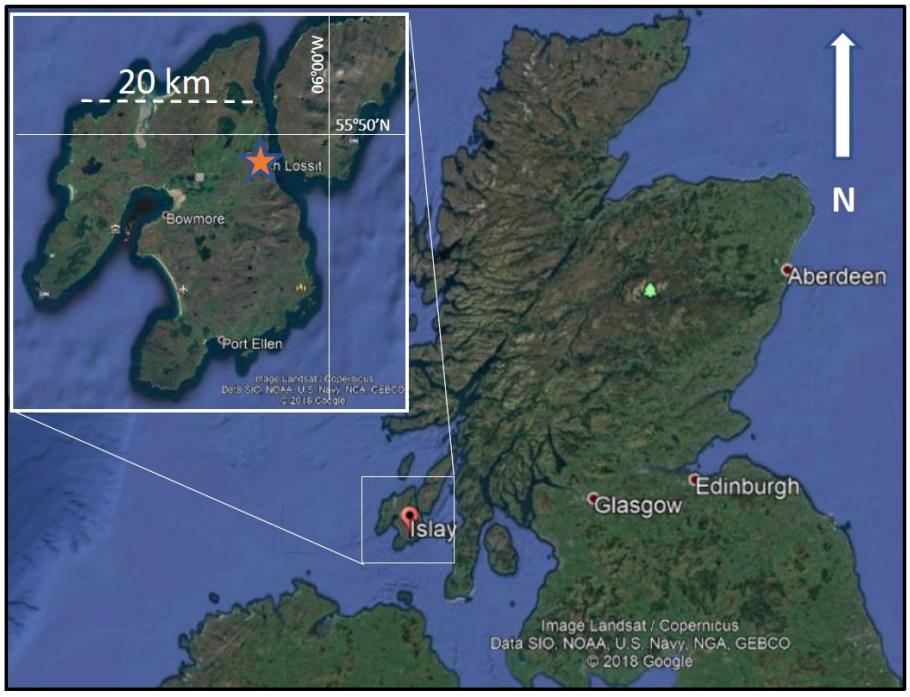

Figure 1. Map showing location of field work concerning the interglacial section of the Port Askaig Formation near Loch Lossit (55°49'N,6°08'W), Islay, Scotland (from Google Earth Pro, 2018).

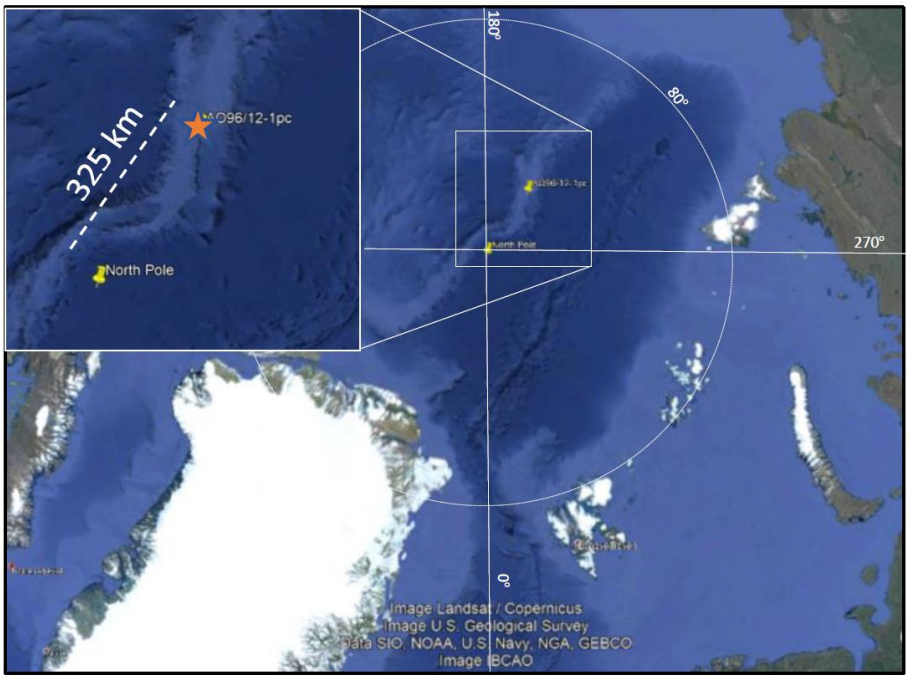

Figure 2. Map showing location where the studied Arctic Ocean sediment core AO96/12-1pc was retrieved (87°05'51''N,144°46'22''E) on the Lomonosov ridge near the north pole (from Google Earth Pro, 2018).

1.2 The Cryogenian Period and the Snowball Earth hypothesis

1.2.1 The Cryogenian Period

The Neoproterozoic Era is defined to start 1000 Ma and end 541 Ma. It followed the Mesoproterozoic and was succeeded by the Cambrian Period. The Neoproterozoic Era consists of the Tonian (1000 – 720 Ma), the Cryogenian (720 – 635 Ma) and the Ediacaran (635 – 541 Ma) Periods (Cohen et al, 2017).

The Cryogenian marks the start of a period with dramatic shifts in the climate with at least two major glaciations, the Sturtian and Marinoan, when the Earth was covered by ice. This is what now is commonly called the Snowball Earth. These two ice ages followed an extended period of more than 1 Ga with seemingly stable climate without detected signs of glaciations. Updated chronology sets the start of the Sturtian glaciation at 717 Ma and ending ca 660 Ma. The shorter Marinoan glaciation is estimated to have had a duration of 5 to 10 Ma with an abrupt ending 635 Ma (Fairchild et al, 2017; Rooney et al, 2015; Hoffman et al, 2017).

The lower level of the Sturtian glaciation is rather well constrained to 717 Ma and with its cap carbonates appearing around 660 Ma. The end of the Marinoan at 635 Ma is also well documented but not its start. It is however evident that there was a longer warm period between the Sturtian and the Marinoan glaciations in the range of 10 – 20 Ma (Fairchild et al, 2016; Fairchild and Kennedy, 2007).

During the Cryogenian continental crust had congregated into one supercontinent called Rodinia, positioned around the equator. Rodinia was built up between 1300 and 900 Ma through tectonic motion. Most likely all continents existing at that time were involved. Rodinia lasted ca 150 Ma. Continental rifting started around 825 Ma, with the first major break-up occurring along the western margin of Laurentia, possibly as early as 750 Ma (Li et al, 2008; Li et al, 2013).

Metazoans were first observed at the very end of the Cryogenian. Evolutionary bottlenecks linked to the recurring Cryogenian Snowball Earth events can have impacted their evolution (Arnaud and Eyles, 2006; Hoffman et al, 1998).

1.2.2 Observations leading up to the Snowball Earth hypothesis

The Cryogenian Period has left many indications of a time with extreme shifts in climate over the entire planet. There are multiple evidence of glaciers reaching sea levels at a time when continents were grouped together at low latitudes in the supercontinent Rodinia. Glacial deposits have been observed in multiple places on all paleocontinents, several of which were judged to have been located at low latitudes at that time (Li et al, 2013). Thirty-nine locations with evidence of glaciations have been dated to the Sturtian glaciation and 48 to the Marinoan (Hoffman et al, 2017). Evidence of the global Sturtian glaciation is found in South Australia, North-West Canada, Greenland, Namibia, Oman, Scotland and South China (Fairchild et al, 2016).

When the climate shifted back to a greenhouse stage, the sudden warming caused calcium carbonate to precipitate, which formed the cap carbonates which are observed in many locations on top of the glacial sediments (Donnadieu and Ramstein, 2002).

Banded iron formations which had been absent since the Great Oxygenation Event in the beginning of the Proterozoic Eon started to reappear during the Cryogenian. There is evidence of the ocean being anoxic and containing free Fe-ions during this time (Hoffman et al, 2017).

The banded iron formations and cap carbonates are two strong indicators of an abrupt end to the Cryogenian global glaciations. (Hoffman et al, 1998).

$\delta^{13}C$ measurements show very strong excursions in carbonate rock just below and above glacial deposits associated with the Cryogenian. Low $\delta^{13}C$ values is interpreted as being caused by drastic reduction in organic life in the oceans. Photosynthesizing cyanobacteria preferably use the lighter isotope and leave the heavier carbon in the water column which give a higher normal $\delta^{13}C$ value in a bio-producing ocean. Records of this are preserved in chemically precipitated carbonate rocks

(Halverson et al, 2010). The carbon isotope data tells a story of a collapse in the photosynthesizing oceanic biota during millions of years, coupled with a global glaciation.

Negative $\delta^{13}C$ excursions have been reported in both the Lossit Limestone below and in the Bonahaven Dolomite Formation above the Port Askaig Formation. Part of the Lossit Limestone anomaly can however be explained by exchange of metamorphic fluids, but the low Bonahaven Dolomite value remain as a strong indicator of a dramatic climatic event (Skelton et al, 2015).

1.2.3 The Snowball Earth hypothesis

J. L. Kirschvink proposed the term Snowball Earth in 1992, based on earlier ideas and modelling by W. B Harland and M. Budyko (Hoffman et al, 1998). The Snowball Earth hypothesis has been further developed and championed by P. F. Hoffman and many other scientists (Hoffman et al, 2017).

The Snowball Earth is a very non-uniformitarian concept, e.g. predicting events that are sudden and are confined to a relatively short geological time-period. In contrast, geological uniformitarianism is based on a gradualistic concept which says that "the present is the key to the past".

At the core of the Snowball Earth hypothesis is an energy-balance model based on two main drivers for climatic change: albedo and CO_2. The model indicates a hysteresis between the loop of the cooling albedo and that of the warming CO_2. Once having passed a certain threshold, the albedo created by the global ice cover will assure that the ice stays despite raising CO_2 from volcanic outgassing. When the CO_2 finally reaches a sufficient level to overcome the albedo, melting will start suddenly. From that point, the reduction in albedo will also work to hasten the climate shift. (Benn et al, 2015).

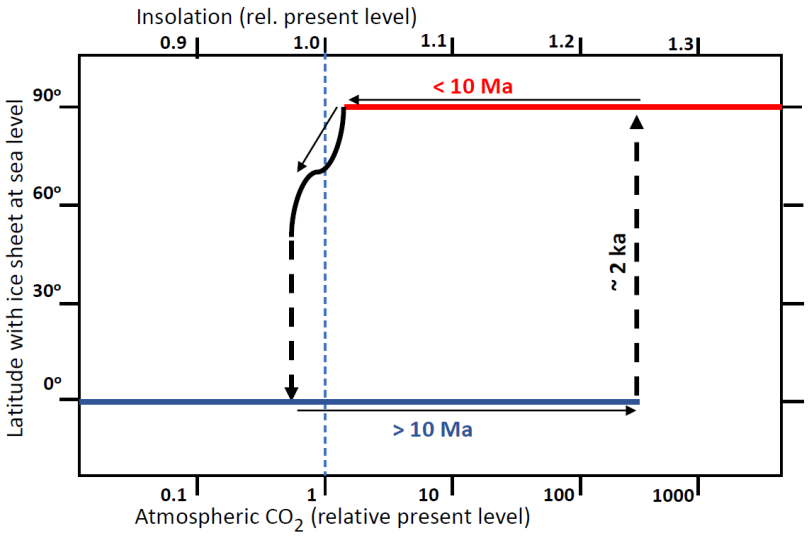

Figure 3. Simplified Snowball Earth energy balance model, redrawn after Hoffman et al (2017). The model indicates two tipping points where 1) build up of ice sheets with increasing albedo, and 2) accumulation of CO_2 in atmosphere from volcanic outgassing, triggers sudden climate shifts from greenhouse to ice house stages and back.

The hydrological cycle will almost come to a stop, chemical weathering will be drastically reduced, biological production in the oceans stops leading to carbon isotope anomalies, ice covered oceans will become anoxic and ferruginous. Cap carbonates will form directly on top of the glacial deposits when the ice cover finally melts after several millions of years. (Fairchild and Kennedy, 2007).

The Snowball Earth is thus created by a runaway albedo feedback leading to equatorial continental glaciers advancing to the sea and oceans being covered by an ice sheet. When ice pass a latitude of ca 30°, the albedo feedback will lead to the full globe being covered by ice. After millions of years with volcanic CO_2 accumulating in the atmosphere up to a level of about 350 times the present one, Earth turns suddenly into an extreme greenhouse condition. Atmospheric carbon transferred into the seas causes rapid precipitation of calcium carbonate building the layer of cap carbonate (Hoffman et al, 1998; Hoffman et al, 2017). Although there are signs of advancing- and retreating glacial ice during the

Sturtian and Marinoan glaciations, this cap carbonate is uniquely linked to the final ice retreat and is also used to constrain the respective termination of these two periods (Hoffman et al, 2017).

A compact ice cover would not only isolate the ocean from atmospheric oxygen and create an anoxic strongly ferruginous deep-sea environment. It would also lead to a reduction of sulphate which has also been observed in carbonates from this period (Hurtgen et al, 2002). Thus, the anoxic Cryogenian ocean not only contains elevated level of free iron but is also low in sulphate concentrations. A snowball ice-covered ocean is however still well mixed with less stratification than the modern ocean. Geothermal heat and cold ice at the surface assures a convection driven mixing of water. The ocean however remains anoxic since the ice cover inhibits atmospheric oxygen from mixing with the water (Hoffman et al, 2017). Re-oxygenation will eventually happen when the atmospheric oxygen is mixed into the water column of ice-free oceans, which creates the banded iron formations.

The Snowball Earth energy balance model predicts this runaway glaciation, but it is not fully clear how Earth would recover from such an event (Fairchild and Kennedy, 2007). Very cold temperatures at the poles could cause CO_2 to freeze, which would be an irreversible sink for this greenhouse gas and not leaving any exit mechanism from the icehouse state (Hoffman et al, 2017).

When the Snowball Earth glaciation terminates after the CO_2 level has built up sufficiently, the climate will rapidly shift into a very warm state. There is however some evidence of orbital forcing in late stages of the Snowball Earth period, which could have worked in tandem with the increased CO_2 greenhouse effect (Fairchild et al, 2016; Benn et al, 2006).

Snowball Earth energy balance models generate one long lived glacial period with continental ice covering low latitudes. The time needed for CO_2 from volcanic outgassing to reach a level where the albedo grip of the climate could be broken is in the range of several million years according to these models. There is a general agreement about the occurrence of low latitude glaciations during the Cryogenian, but the continuous length of these glaciations is less certain (Li et al, 2013).

The initial trigger for glaciation with the albedo feed-back driving the Earth into a Snowball Earth stage is not clear. Greenhouse CO_2 drawdown caused by extreme chemical weathering linked to the erosion of low altitude Rodinia has been proposed as one mechanism for this (Rooney et al, 2015; Fairchild & Kennedy, 2007).

Collapse of single cell life with reduced organic production during the Snowball Earth plus a pulse of very extreme chemical weathering afterwards are normally used to explain the $\delta^{13}C$ excursion in the cap carbonate which followed the glaciation.

The Snowball Earth hypothesis generates certain predictions that can be tested. If the model gives an accurate description of the process, then the glaciations shall start and end globally at the same time, and the length of one glaciation cycle shall be in the order of several million years (Rooney et al, 2015). The first prediction seems to hold true, where glacial deposits found on several different paleo-continents have been age constrained to the same Sturtian period (Rooney et al, 2015). However, the second prediction of a multimillion year glacial cycle has been difficult to verify. Sequences of tillite intermixed with non-glacial mud- and sandstone, e g in the Port Askaig Formation (Ali et al, 2017), rather seem to contradict this required result from the Snowball Earth hypothesis. The Port Askaig Formation contains ca 47 tillite diamictite horizons which have been estimated to have been deposited over a period of ca 10 Ma (Ali et al, 2017) and which would imply an average glacial-interglacial cycle of ca 200 ka.

The predictions of the Snowball Earth hypothesis are in contradiction to processes observed in the current Quaternary ice age, where continental ice sheets primarily build up and decay in the Northern Hemisphere and where cycles have lengths in the range of 100 ka.

When raising CO_2 levels finally triggered a rapid melting of the snowball ice within a few ka, sea levels would rapidly raise with a magnitude in the range of 0.2 to 1.0 km. Other factors such as isostatic rebound would operate on similar time scales, but expanding warmer sea water would take considerably longer time before adding another 40 to 60 m (Hoffman et al, 2017).

1.2.4 Alternative explanations

There is contradictive evidence in the diamictite records of shorter multiple glacial-interglacial cycles, and with glaciogenic material deposited into open oceans. Thick and well preserved alternating sediment-layers indicate cycles of ice-free and ice-generated depositional conditions, which is not compatible with the Snowball Earth model (Arnaud and Eyles, 2006).

Observed cycles of marine regressions and transgressions are not compatible with a snowball Earth model which produce a rapid transition into a full glaciation, limited activity during the frozen state, and a rapid exit when sufficiently high CO_2 levels triggered a return to a greenhouse state (Fairchild and Kennedy, 2007; Le Heron et al, 2011). These series of sea level transgression and regressions do not correlate with a low speed hydrological cycle during a Snowball Earth (Benn and Prave, 2006). The original hypothesis is not anymore thought to provide the full answer (Klaebe et al, 2018).

Alternative explanations have been proposed, but none seems to provide a complete answer to all characteristics of this extreme period.

The Slushball Earth alternative handles evidence of equatorial glaciation during well constrained and extended periods as well as evidence of an active hydrological cycle with at least temporarily open oceans. Modelling a Slushball Earth does not easily produce stable states with equatorial glaciation leaving an open sea (Fairchild and Kennedy, 2007). It does not either provide predictions that have been possible to verify or falsify (Fairchild and Kennedy, 2007).

The so-called Zipper-Rift Earth hypothesis posits glaciers on uplifted rift-shoulders at low latitudes, but give limited correlation with observed phenomena (Fairchild and Kennedy, 2007).

The High-Tilt Earth hypothesis (Fairchild and Kennedy, 2007) provides yet another alternative explanation for low latitude Neoproterozoic glaciations. A high obliquity of Earth's axis would lead to possible glaciations at the palaeoequator but would still allow for an active hydrological cycle and open oceans. However, there is no evidence for such a shift in Earth's tilt, nor any mechanism proposed for how to recover from this stage (Donnadieu and Ramstein, 2002).

Tziperman et al (2011) have proposed a biological mechanism where an abundance of larger eukaryotic phytoplankton would be responsible for the transport of carbon into a deep anoxic ocean, and where it would undergo remineralization via sulphate- or iron-reducing bacteria. The reduction in atmospheric CO_2 would thus have been the main trigger for the large glaciations and would also explain the carbon isotope excursion at the beginning of the glaciation as being uncoupled from the snowball earth processes. A subsequent oxygenation of the oceans would have prevented a repetition of the Snowball Earth during later Phanerozoic times.

Some more dubious alternative hypothesises include explanations of observed diamictite as being bolide ejecta, and a non-dipole magnetic field at the Neoproterozoic having distorted paleomagnetic assessment of latitudes (Ruddiman, 2014).

Some climate-models have been developed that may allow water belts in low latitudes, despite the runaway effect of the albedo. The Cryogenian ice ages would be expected to follow similar patterns as the present Quaternary ice age with alternating glacial and interglacial cycles and with the same complex interactions of drivers and feed-back mechanisms. This would be a necessary ingredient in a Slushball Earth scenario, but most models are only able to create unstable solutions risking falling into the full Snowball scenario (Hoffman et al, 2017).

All in all, the Snowball Earth hypothesis gives the most comprehensive explanations and applies a multidisciplinary Earth System Science perspective, integrating different processes into the model, even if several types of observations remain unexplained.

The original hypothesis generated certain predictions, which were testable, and which lead to certain modifications of the hypothesis (Fairchild and Kennedy, 2007). Hoffman et al have in their 2017 paper not only summarized these certain problematic observations and processes that would contradict the original Snowball Earth hypothesis, but have also outlined several explanations and modifications to the modelling of the snowball Earth system which would address these issues. The originally postulated shut-down of the hydrological cycle is now assumed to allow a net accumulation of ice at ca 20^{o} latitude and a net sublimation at the equator, leading to gravity induced ice flows. Although the ocean is thought to be covered by ice, meteoric water would still allow some oxygenation in silled basins and fjords, explaining the early occurrence of synglacial ironstones. Certain climatic energy models would allow the existence of ice-free terrestrial areas which i.a. could explain the subaerially formed polygonal sand-wedges observed in 13 diamictite layers within the Port Askaig Formation.

1.3 Port Askaig Tillite Formation

1.3.1 Short geological history of Islay and overall stratigraphy

Islay has a geological record covering the last 1800 Ma. The oldest rocks are found in the Rhinns Complex, which was added to the continental crust with accretion of island arcs ca 1700 Ma. The Colonsay sedimentary rocks were added around 750 Ma when Rodinia were starting to rift apart. The Lossit Limestone, Port Askaig Tillite and Bonahaven Dolomite Formations give evidence of dramatically shifting climates, covering the time from just before until just after the Sturtian glaciation ca 720 – 660 Ma (Ali et al, 2017). These are followed by the Jura Quartzite deposited in shallow oceans and by the Port Ellen Phyllites as sediments in an opening Iapetus ocean ca 600 Ma. When the same Iapetus ocean started to close, the Caledonian orogeny metamorphosed and folded much of the rocks on Islay around 470 Ma. Swarms of basaltic dykes cut through and intruded existing rocks when the Atlantic sea started to open ca 55 Ma. Finally, much of the surface of the island was reworked during the last 2.6 Ma of Quaternary glaciations (Webster et al, 2017.)

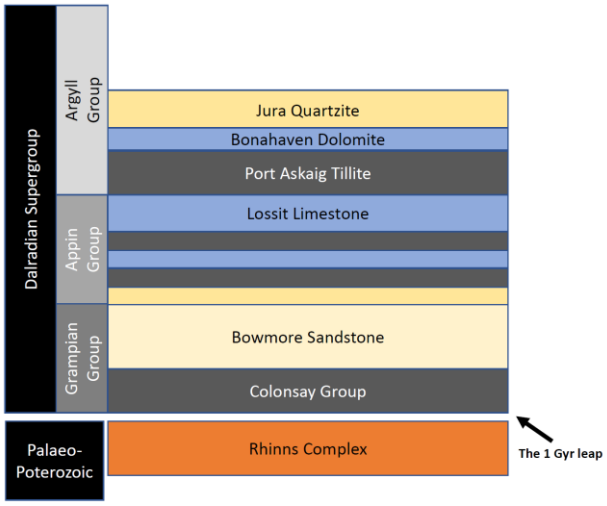

Figure 4. Stratigraphy of the Dalradian Supergroup, redrawn after Webster et al, 2017.

The Rhinns Complex being the base of Islay is built of igneous felsic and mafic rocks. These rocks have a calc-alkaline composition, indicating a magma coming from a depleted source from below an island arc. Rocks of similar composition are also found in Sweden, Canada and Greenland, indicating a similar origin. It is believed that this island arc was accreted to the Archean province about 1700 Ma, at which time the rocks

underwent metamorphosis into amphibolite facies. Same island arc accretion also built large parts of the continental crust in Sweden during the Svekofennian orogeny (Webster et al, 2017).

Nothing remains of the geological history from the Meso-Proterozoic. Rocks from the Colonsay Group with an approximate age of 750 Ma lays above the Rhinns Complex. This rock was formed by sedimentation in extensional basins formed during the rifting of Pangea supercontinent and contains sandstone and turbidites. This rock was later metamorphosed at greenschist facies conditions at a temperature of 350 – 550^{o}C and a depth of 6 – 30 km (Webster et al, 2017).

At some time after the build-up of the Colonsay Group, a sequence of limestone was formed which is called the Lossit Limestone Formation. This limestone was precipitated in a warm tropical and shallow sea environment, as is evidenced by the occurrence of stromatolites. Directly on top of this limestone, the Port Askaig Tillite is found, which contains limestone and granite clasts as well as drop-stones. It has been linked to the Sturtian glaciation ca 717 – 660 Ma. Within the Port Askaig Tillite Formation, layers of extremely iron-rich rock are found which indicate precipitation of Fe-oxides during a sudden oxygenation event (e g where a global ice sheets suddenly melts). Within and on top of this formation, pseudomorphs of polygonal frost wedges and frost-shattered stones are found, which indicates a periglacial environment above the water surface (Ali et al, 2017; Hoffman et al, 2017; Webster et al, 2017).

Above the Port Askaig tillite, a dolostone layer is found. Assuming that the Port Askaig Formation is Sturtian, the age of this dolostone layer is thus younger (<660 Ma). This rock is interpreted as a cap carbonate which is expected to form directly after a global glaciation event. This dolostone is named the Bonahaven Dolomite Formation and contains several indicators of a warm tropical climate with sedimentation in a shallow sea, including an abundance of stromatolites, biofilms and pseudomorphs of anhydrite (evaporitic deposits with gypsum). It however also contains indications of aragonite which normally is an indicator of colder seas, but which also can be explained by rapid weathering. Above the Bonahaven Dolomite, a thick layer of quartzite is found which is named the Jura Quartzite Formation. This is also deposited in a relatively shallow sea and is younger than the Bonahaven Dolomite. Both the Jura Quartzite and the Bonahaven Dolomite were metamorphosed and folded during the Caledonian orogeny ca 470 Ma. The fold forms an anticline in North Islay, and which is cut through by a fault with a zone of breccia which was formed thereafter (Webster et al, 2017).

During the opening of the Iapetus ocean ca 600 Ma, sediments were deposited in the spreading ocean. Between these sedimentary rock layers intrusions of basaltic sills came in. The full sequence was later metamorphosed into greenschist facies and tilted during the Caledonian orogeny ca 470 Ma, forming phyllite and meta-basalt (Webster et al, 2017).

The Palaeozoic and Mesozoic (541 – 66 Ma) period was rather uneventful with little remaining evidence in the geological record on Islay. The rifting for the Atlantic sea started around 60 Ma and numerous basaltic dykes from around 55 Ma are seen to cut through rock layers on Islay (Webster et al, 2017).

During the Quaternary Period Islay has seen several severe glaciations with warmer inter-glacials in between. Each of these waves of glaciation eroded and reworked the landscape, leaving very little evidence from the preceding glaciation. Thus, the quaternary landforms and depositions on Islay are mainly from the Last Glacial Maximum (LGM) up to the present day. The LGM was ca 30 – 25 ka ago at which time the ice sheet over Islay was ca 500 m thick. The ice started to retreat from Islay about 20 ka, and it is estimated that this area was ice-free ca 16 – 15 kA. The flow of the ice and its subsequent

melting during its retreat resulted in numerous quaternary depositions and landforms still seen on Islay today (Dawson, A.G., 1984; Webster et al, 2017).

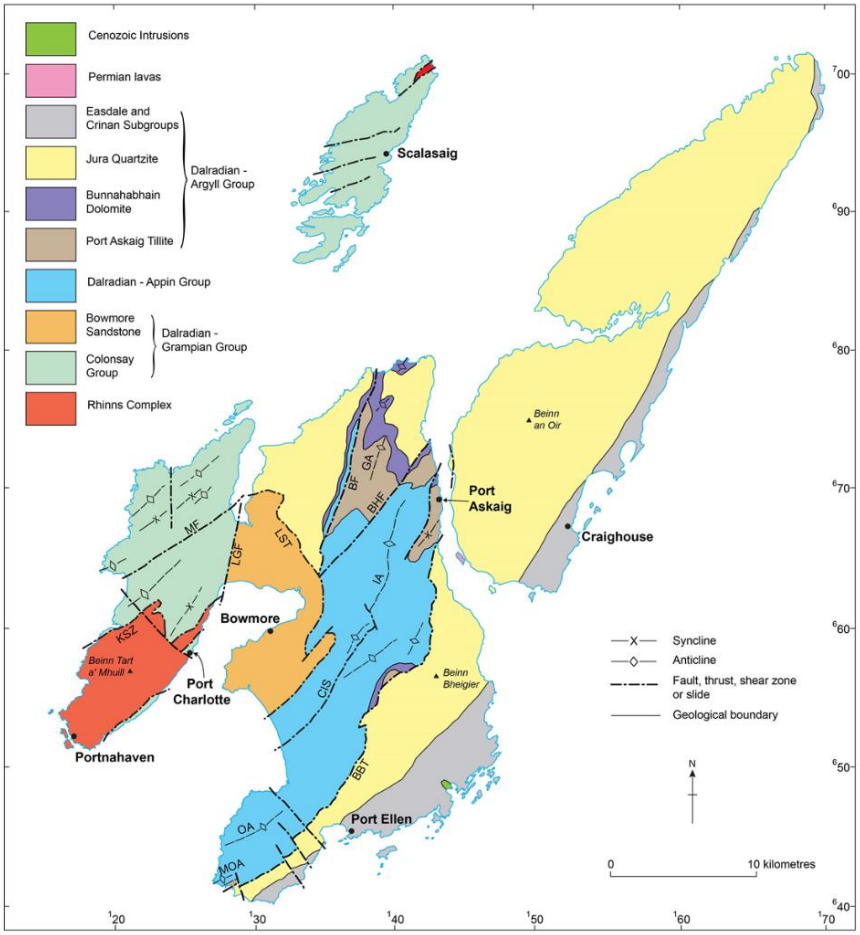

Figure 5. Geological map of Islay (Webster et al, 2017).

1.3.2 Port Askaig Formation – age and paleogeography

The lower units of the Port Askaig tillite are missing on Islay, which either indicates an unconformity or that the underlaying layers are not laterally continuous here. Above the Port Askaig a cap carbonate is found, called the Bonahaven Dolomite. (Arnaud and Eyles, 2002). There is however a thicker clastic sequence deposited in an intertidal marine setting inserted between the tillite and the cap carbonate, which creates some uncertainty as to the interpretation of this dolomite layer (Skelton et al, 2015; Prave et al, 2009).

The Port Askaig Formation is believed to have been formed during the start of the Sturtian glaciation (Arnaud and Eyles, 2002). Also, Benn and Prave (2006) conclude with this time of ca 720 Ma. However, this date can be questioned since it would imply a quite extended period of extensional rifting before Iapetus Ocean opened (Arnaud and Eyles, 2006).

$\delta^{13}C$ measurements of Lossit Limestone and Bonahaven Dolomite Formation have been corelated with other global carbonate data, which place the Port Askaig Formation well within the time of the Sturtian glaciation (Prave et al, 2009).

Islay was located at the rift zone between Baltica and Laurentia at southern subtropical latitudes during the Cryogenian Period., The estimate of the latitude at the start of the Sturtian varies between ca 30° S (Benn and Prave, 2006) to ca 20° S (Hoffman, et al, 2012). According to a global reconstruction of paleocontinents made by Li et al (2013), it was located at semitropical latitudes ca 25° S at 720 Ma and

somewhat further south ca 30° S at 680 Ma. At the end of the Marinoan 635 Ma it had moved to ca 45° S. These reconstructions are however uncertain and not very well constrained (Arnaud and Eyles, 2006; Fairchild and Kennedy, 2007). The occurrence of glacial deposits at low equatorial latitudes at numerous different paleocontinents is however not anymore disputed.

1.3.3 Port Askaig Formation – stratigraphy

The Port Askaig Formation is ca 1100 m thick and is divided into 47 diamictite beds, which are grouped into 5 members. It is seen in 30 localities from NE Scotland to W Ireland but most prominently on the Garvellach Islands and Islay. These five members have different clast lithologies, with the bottom (Member I) primarily containing dolostone clasts from the underlaying Lossit Limestone (Ali et al, 2017; Eyles, 1988). Clasts in successively higher members becomes more and more granitic silica-rich and are not plucked in situ (Ali et al, 2017).

Member I contains stacked beds of diamictite, mudstone and sandstone, but no periglacial structures (Ali et al, 2017). The mudstone occasionally contains examples of dropstones, as was also observed on site during XRF data collection. Member I also includes two atypical diamictite layers. The first, the Great Breccia, contains very large matrix-supported clasts of dolostone within a dolomitic matrix with varying thickness. On the Garvellach Island it is ca 40 to 50 m thick while becoming thinner to the southwest with ca 4 m on Islay. (Eyles, 1988; Benn and Prave, 2006).

Overlying the Great Breccia is another distinct sequence called the Disrupted Beds, containing detrital dolostones and mudstones with a very high Fe-content. The Fe is oxidized to hematite and some siderite. Its matrix has a characteristic dark blue colour and it shows soft sediment deformation features. (Arnaud and Eyles, 2002; Benn and Prave, 2006). The Disrupted Beds contain occasional dropstones (Eyles, 1988).

Figure 6. The Disrupted Beds visible in outcrop near Loch Lossit, Islay (photo by author, 2018)

The diamictite layers normally have distinct basal contact with conformable underlaying sandstone, dolostone or mudstone (Ali et al, 2017; Eyles, 1988). There is no evidence of erosion at these diamictite bases. There are examples of tidal sandstones in between the diamictite beds. (Ali et al, 2017). The upper surface of the diamictites contain frost shattered clasts and sandstone downfolds which is interpreted as periglacial structures. This indicates a succession of glacial-nonglacial deposits which occasionally have been located in a subaerial environment. (Ali et al, 2017).

The Lossit Limestone was deposited in a low energy environment on a continental shelf, and the Bonahaven Dolomite in a shallow marine or lagoon environment (Arnaud and Eyles, 2002).

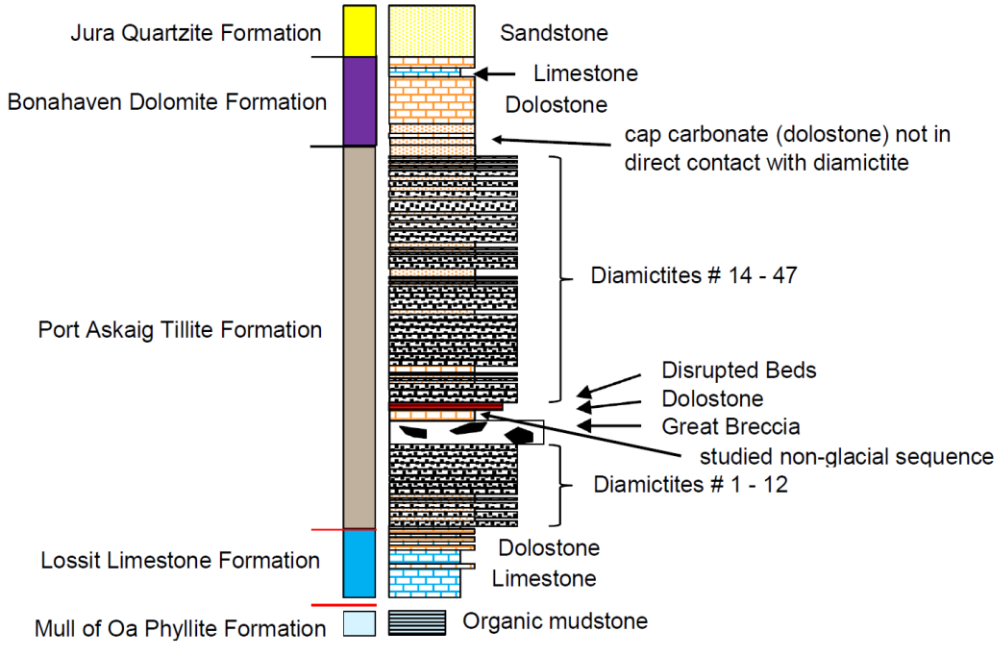

Figure 7. Port Askaig stratigraphy, including underlaying and overlaying formations (from personal communication Alasdair Skelton, April 2018).

1.3.4 Tectonic setting for the build-up of the Port Askaig Formation

The tectonic setting for the Port Askaig Formation is characterized by processes resulting in the initial opening of the Iapetus ocean. This included an unstable tectonic environment with rifting and extensional basins forming, with faulting of listric type. The tectonic setting for the build-up of the Port Askaig Formation was thus an extensional environment containing fault-bounded blocks and shallow basins created by the rifting (Arnaud and Eyles, 2002).

During the Caledonian orogeny ca 460 – 480 Ma the Port Askaig Formation had been weakly metamorphosed to greenschist facies. On Islay this reached a maximum pressure of ca 1 GPa and temperature between 410 – 470 °C (Skelton et al, 1995 cited in Fairchild et al, 2017).

This continental basin was subject to a relatively fast subsidence which kept pace with sedimentation filling it up (Fairchild et al, 2017). However, during the extreme climatic variation of the Sturtian glaciation, this area must have experienced several sea-level changes caused by isostatic adjustment and waves of meltwater (Ali et al, 2017). Overall sedimentation rate has been estimated to be around 100 – 125 m/Ma, and Port Askaig Formation was thus formed within a limited period of about 10 Ma (Ali et al, 2017).

1.3.5 Possible depositional mechanisms and paleoenvironment

There has been disagreement concerning the interpretation of the paleoenvironment conditions under which the Port Askaig diamictite layers were deposited. Interpretations cover everything from subglacial till from grounded ice, or glacimarine deposits at the ice margin, to a marine slope deposit without glacial processes (Fairchild and Kennedy, 2007).

The first 12 diamictite horizons are most commonly thought to be deposited in a glaciomarine environment as ice rafted debris, suspension rain-out and with some dropstones. The 13th horizon, being the Great Breccia, is by some believed to be a pro- or subglacial till with glaciotectonite features

and by others a massive debris flow from a collapsing carbonate platform. The last horizons from 14 – 47 are again likely to be of glaciomarine origin.

Comparison with Quaternary examples give one interpretation of the Great Breccia as a proglacial deformation of a shallow carbonate platform caused by advancing grounded ice. Large folds and other deformation structures makes it similar to a Quaternary proglacial trust moraine (Benn and Prave, 2006). In a similar fashion, the Disrupted Beds are compared with subglacial deformations. It has several features characteristic for glaciotectonite which has been deformed but kept some of its original structure including rigid boudins and inclusions of exotic clasts indicative of ice rafting (Benn and Prave, 2006).

As an alternative, it has been proposed that the Great Breccia was formed by subaqueous debris flows caused by catastrophic failure of a carbonate platform, collapsing because of earthquakes (Arnaud and Eyles (2002). The Great Breccia resembles other megabreccias formed in deep water marine settings as result of collapsing carbonate platforms. The Disrupted Beds have also been attributed to the rifting and extensional faulting which lead to the subsidence of the Dalradian Basin during a period of tectonic instability (Arnaud and Eyles, 2002; Eyles, 1988). According to this hypothesis, there is no reason to believe that a glacial process was involved in the formation of these layers (Arnaud and Eyles, 2002). In this alternative proposal, the Port Askaig Formation is interpreted as an overall shallowing upwards sequence. The material in the diamictite layers is primarily generated during transgressive periods by ice rafted debris, suspension rain-out and fine-grained sediments settling out of the water column, while the sandstone layers are deposited during regressive periods in a tidally dominated shallow marine environment. (Eyles, 1988; Arnaud and Eyles, 2006). It shall however be noted that there are 12 beds of tillite of clearly glacial origin below the Great Breccia (Ali et al, 2017) which do not fit well with this interpretation.

A better understanding of the depositional mechanisms for the Port Askaig diamictite horizons and its paleoenvironment will lead to a more exact interpretation of the climatic changes and global ice-cover during the Sturtian glaciation and could ultimately have a bearing on the validity of the Snowball Earth hypothesis. Certain questions remain unanswered and are intensely debated among scientists. This include i.a.:

- to what extent the mass movements were controlled by tectonic or climate factors – that is partly by gravity flows triggered by earthquakes or only by glacial processes
- the transport mode for glaciogenic diamictite material – by grounded ice or by ice rafting
- the number and length of the glacial-interglacial cycles – where the classical Snowball Earth hypothesis would require cycles in the order of Ma, while an orbital solar controlled process would imply cycles in the order of 100 ka or lower
- the depositional environment – marine or lacustrine and shallow subaqueous or even subaerial

Based on the literature review presented in this Introduction and Geological Framework section and interpretation of results from the analysis of an interglacial sequence from the Port Askaig Formation on Islay, these questions will be addressed in the Discussion section of the report.

1.4 The Arctic Ocean during the Quaternary and its sedimentation environment

1.4.1 The Quaternary Period

The Quaternary Period is defined to have started 2.58 Ma and continues until present time. It includes the Pleistocene and the current Holocene epoch. (Cohen et al, 2017). The Quaternary is characterized by cycles of glaciations interrupted by shorter interglacials. The Earth moved into this ice age already

34 Ma ago at the beginning of the Oligocene when the Antarctic ice sheets were established, but it is during these last 2.6 Ma that the northern hemisphere has been covered by large continental ice sheets (Ruddiman, 2014).

The marine benthic $\delta^{18}O$ record is an excellent proxy to follow the glacial cycles. The lighter ^{16}O accumulates in continental ice sheets, and leaves the oceans enriched in ^{18}O. It is thus primarily an indicator of the ice volume, i.e. the stage of glaciation. $\delta^{18}O$ record shows large oscillations in continental ice sheets throughout the Quaternary with ca 50 glacial-interglacial cycles during this period. These oxygen isotope cycles (called Marine Isotope Stages or MIS) have been numbered with odd numbers indicating interglacials and even numbers glacials (Zachos et al, 2001; Lisiecki & Raymo, 2005).

The Quaternary is characterised by repeated and regular widespread glaciation of the northern hemisphere. The Last Glacial Maximum (LGM) was ca 26.5 – 19 ka (Clark et al, 2009) and we are now in the most recent interglacial period. The glacial periods impose major changes in Earth's climate (Ruddiman, 2014).

The ice sheet grows or shrinks as a function of ice accumulation and ablation. The ice flows from areas of net accumulation to areas of net loss. On the way it erodes, deforms, transports and deposits substrate material. This leaves numerous geological evidence of ice sheets, both as glacial sediments and in landforms as well as in the oxygen isotope excursions. The large mid-latitude continental ice sheets during Quaternary glaciations lead to large relative sea level changes. These changes are the combined effects of a global decrease in ocean volume (eustatic sea level decline) and isostatic depression. The sea level is estimated to have been ca 134 m lower during the LGM (Lambeck et al, 2014).

Average $\delta^{18}O$ values shows a steady increasing trend during the Quaternary indicating additional cooling and expanding ice sheets (Zachos et al, 2001; Lisiecki & Raymo, 2005).

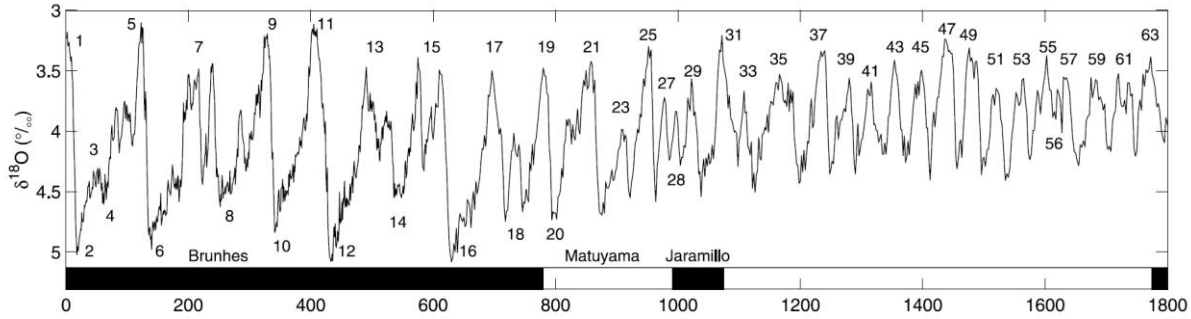

Figure 8. Lisiecki, L.E. & Raymo, M.E., 2005, A Pliocene-Pleistocene stack of 57 globally distributed benthic $\delta^{18}O$ records, which show both an overall trend towards larger $\delta^{18}O$ values as well as increasing amplitudes.

The Quaternary glaciations show a characteristic sawtooth pattern with an asymmetric longer build-up of continental ice sheets in the Northern Hemisphere, followed by rapid deglaciations. During the last 900 ka this has occurred with a periodicity of ca 100 ka, while the period was shorter (closer to 40 ka) in the earlier part of the Quaternary. There is an obvious correspondence with the Milankovitch cycles, with an obliquity of 41 ka and a main precession cycle of 23 ka. However, the mechanism between solar forcing and ice mass development does not seem to be linear. Other processes such as change in atmospheric and ocean circulation and especially deep-sea storage of CO_2 are most probably coupled to this (Paillard, 2015).

It is also clear that the Quaternary climate and global environment is not comparable with the Cryogenian Period, as evidenced by the glaciation of tropical platforms (Li et al, 2013) and anoxic and ferruginous chemistry of the oceans at that time (Hood and Wallace, 2014).

1.4.2 The Arctic Ocean

The Arctic Ocean has certain characteristic features. It is relatively small and is surrounded by continental land masses providing limited connections to other oceans. The Arctic Oceans location at the North Pole gives it a key position in forming the global climate and it has played a vital role in the Quaternary glaciation cycles when it has been fully or partly covered by sea ice and ice shelves (Jakobsson et al, 2014).

A relatively large part (ca 53%) of the Arctic Ocean consists of shallow continental shelves (Jakobsson, 2002). It is surrounded by continents with rivers draining large inland areas, delivering diverse types of sediments into the deeper sea bottoms. Surface currents direct the flow of iceberg and sea ice which are the main vehicles for transporting sediments of continental origin. Sea ice is the most important vehicle for the transport of clastic components during interglacials, while icebergs become more important during glacial periods (Bischof, 2000 cited in Sellén et al, 2010). Since the Lomonosov Ridge is higher than the surrounding sea floor, it should not have been impacted by turbidity. Sediment particles with an origin from the continents should therefore have been deposited by ice rafting, i.e. sea ice or floating ice bergs. (Jakobsson et al, 2001).

Manganese variations in central Arctic Ocean is believed to be linked to run-offs from the large Siberian rivers which pass through extensive areas with peat bogs and boreal forests, combined with contrasts in ventilation of the ocean waters. Output from these rivers was probably strongly dependant on the glacial- interglacial cycles. (Jakobsson et al, 2000). Manganese variations in sediment cores is a good proxy for climate change in the Arctic Ocean setting.

The Arctic Ocean was probably covered by continuous ice shelf with an approximate depth of 1000 m during the Marine Isotope Stage 6 ca 140 ka ago (Jakobsson et al, 2016). This ice shelf was of nearly uniform thickness and grounded on the Lomonosov Ridge and possibly on other bathymetric heights. Plowmarks and eroded sediment layers on the Lomonosov Ridge are believed to be caused by the ice shelf down to ca 1000 mbsl (Jakobsson et al, 2016; Nilsson et al, 2017). In contrast to the Antarctica where the ice shelves always have terminated in open sea during the Quaternary, the Arctic Ocean was at this time constricted by continents covered by glaciers with only a smaller outlet for the ice between Greenland and Svalbard. This resulted in a back-stress which supported and stabilized km-thick ice shelves with limited variations in thickness. This is what allowed the uniform ice shelf to develop, and there are also some analogies that can be drawn with the possible ice dynamics of a Snowball Earth. An ice shelf system is inherently dynamic and will not be stable, but a globe completely covered by ice with no outlet for moving ice shelves would correspondingly have allowed a thicker continuous ice shelf to be built up (Nilsson et al, 2017).

Can the glacial history of the Arctic Ocean be compared to the Snowball Earth in other ways? The sediment cores of the Arctic Ocean have revealed its past 1 Ma history of glacial-interglacial cycles. Marine-based ice sheets and ice shelves have developed during the cold periods and decayed during the warm, covering all or part of the sea surface. Influx of warmer Atlantic water took place at deeper levels during the glacial periods, which lead to reduced basal melting of the ice shelves. Ocean circulation and oxygenation have changed in tandem with this. (Jakobsson et al, 2014). The overall cycle was forced by Milankovitch cycles with insolation forcing working together with albedo and CO_2 feed-back mechanisms. During maximum glaciation when the sea level was more than 100 m lower

than today, Bering Strait was closed, and freshwater circulation was almost stopped. This reduced the hydrological cycle, which possibly mimic a Snowball Earth situation (Jakobsson et al, 2014).

The tidal impact is small within the limited area of the Arctic Ocean but can probably not be neglected in a completely ice-covered and isolated Snowball Earth ocean. The ice cover would be subject to mechanical stress and the gravitational energy from tidal forces could play a part in the overall energy balance, as it clearly does in the energy balance of the ice-covered moons of the larger planets in the solar system.

Examples of ice shelves protruding from the continental ice sheets into open ocean are also found in Antarctica. The West Antarctic Ice Sheet is grounded at the sea bed and is feed by ice streams into floating ice shelves. The mass balance of the ice shelf is strongly dependent on water temperature and water circulation. In certain models the ice shelf has been assumed to be thinning with ca 5 m for each km it extends from the grounding line (Jakobsson et al, 2010). The mass balance of an ice shelf is primarily impacted by basal melting. Oceanic temperature and vertical mixing are therefore leading components in the mass balance of today's Antarctic ice shelves (Nilsson et al, 2017). Since the Snowball Earth ocean was well mixed (Hoffman et al, 2017), it is however not evident how and when this system reached an equilibrium with the geothermal heat flow.

1.4.3 Transport mechanisms and sedimentary regimes of glaciogenic materials

There are three mechanisms for transport and deposition of glaciogenic material (personal communication, Sarah Greenwood, March 2018):

i. Subglacial transport producing till, often with glaciotectonic structures
ii. Glaciofluvial transport, producing better sorted material such as sand and gravel
iii. Glaciomarine transport, producing ice rafted debris, suspension rain-outs and dropstones in marine (and lacustrine) environments

Glacial ice is an effective transporter of till when it is warm based, but much less so if cold based (Ruddiman, 2014). The diamictite layers thus presuppose that the Snowball Earth climate still allowed basal melting of the glacial ice for the glaciogenic deposits to have been formed.

The sedimentation rate is typically high at the ice-margin. In ice covered areas it primarily consists of basal melting of the sea ice and transports by currents (Jakobsson et al, 2014). Sea ice rafted debris transported by the Transpolar Drift is presently the main supplier of sediment to the Lomonosov Ridge, with periods of iceberg transport in the past (Sellén et al, 2008). Since the content of coarse fractions (>63 µm) has decreased during the Holocene, most sediment transports have been by sea ice with little contribution from icebergs (Sellén et al, 2008). The sedimentation rates under the ice margin (reflecting seasonal changes over longer periods) is higher than for ice-free areas, and the rates are lowest under permanent ice. (Hebbeln and Weffer, 1991, cited in O'Regan et al, 2008)

Intensive work has been done trying to establish a common stratigraphy for Arctic Ocean sediment cores. It is still challenging to age-calibrate marine geological records from central Arctic Ocean to correlate those with glacial cycles. For older sediments beyond 200 ka the most common methods include bulk density and magnetic properties of the sediments, which appear to be the most reliable proxies mirroring the Milankovitch cycles of glacial and interglacial depositional environments (O'Regan et al, 2008). Different indicators of physical properties such as colour, paleomagnetism, optically stimulated luminescence, biostratigraphy and density content of coarser grains (Sellén et al, 2008) have been used.

Based on an Arctic Ocean sediment core identified as AO96/12-1pc collected in the 1996 Arctic expedition, Jakobsson et al (2000) constructed an age model based on nannofossils, manganese and colour cycles being correlated with a $\delta^{18}O$ stack from Bassinot et al (1994). Certain analysis of content of chemical elements using ion coupled plasma atomic emission spectroscopy (ICP-AES) and XRF scanners have also been done on this same core. The sediment structure of AO96/12-1pc covers a series of cold and warm periods.

Based on presented age-model for the 96/12-1pc core, the first 110 cm up to 52 ka has a sedimentation rate of ca 2.8 cm/ka, while the remaining deeper section up to ca 858 ka has an average of ca 0.5 cm/ka (Jakobsson et al, 2000; Jakobsson et al, 2003). However, there is evidence of faster sedimentation during parts of the glacial-interglacial cycles with abrupt environmental changes. The sedimentation rates have been re-confirmed by optically stimulated Luminescence (OSL) dating (Jakobsson et al, 2003). The sedimentation patterns however differ in various parts of the Arctic Ocean, where the Amerasian Basin shows slower deposition rates as compared to the Eurasian Basin (Sellén et al, 2008). A sedimentation growth of above 1 cm/ka seem likely also for older sediments within the Arctic Ocean area (O'Regan et al, 2008).

The Antarctica Western Ross Sea region shows a similar sediment structure as is seen in the Port Askaig Formation. Drilling has revealed more than 1000 m thick layer of glacial-interglacial sediments representing a time of 34 Ma. The drill cores reveal sequences of facies from pelagic open water deposited mudstone, to current or wave transported sandstone, to sub- or proglacial diamictite (Dunbar et al, 2008; Wilson et al, 2012). Although the diamictite beds can be produced by different glacimarine processes such as meltwater outwash, melt-outs and proglacial debris-flows, these have been interpreted as basal till produced by grounded ice (Wilson et al, 2012). Typical of this cycle from grounded ice to glaciomarine to open sea are disconformities associated with the diamictite beds. This represents erosion surfaces caused by the advancing grounded ice, truncating underlaying layers. There are at least 49 separate diamictite beds observed and a similar number of erosional surfaces (Dunbar et al, 2008; Wilson et al, 2012; Ali et al, 2017). Similar observations come from drill cores in the East Antarctica Victoria Land basin where 46 erosional unconformities were noted within the glacimarine cycles of ice-margin advance and retreat (Naish et al, 2001). Diamictite beds combined with erosional surfaces thus seem to be a hallmark of pro- and subglacial till deposited by grounded ice.

An age models for Western Ross Sea implies an overall relatively rapid sedimentation rate of 20 – 50 cm/ka, including the diamictite beds and as adjusted for erosional surfaces (Wilson et al, 2012). A more constrained section at about the Oligocene/Miocene boundary implies an overall sedimentation rate of 12 cm/ka (Dunbar et al, 2008).

1.4.4 Milankovitch orbital forcing of climate change

$\delta^{18}O$ data undoubtedly shows that growth and decays of Quaternary ice-sheets are paced by Milankovitch orbital cycles (Lisiecki & Raymo, 2005). Shifts in Earth's eccentricity, obliquity (tilt) and precession create varying solar influx of energy. These primarily combine into 41 and 23 ka cycles (Ruddiman, 2014).

The orbital paced rhythms of the glaciation cycles during the Pliocene – Pleistocene have varied around a long-term trend towards cooler climate. This longer trend is assumed to be driven by tectonics (continental geography and orogenetic induced weathering) and CO_2 levels (Zachos et al, 2001). Orbital control in this period has primarily been of the obliquity type with cyclicity of 41 ka and which is most effective at high latitudes (Dunbar et al, 2008). The eccentricity component has quite a small impact

on total insolation. The third orbital factor being precession is normally modulated by eccentricity and has a combined cycle of ca 23 ka. This is primarily having effect at lower latitudes. (Zachos et al, 2001).

The current ice age shows gradual build-ups of ice sheets during the glaciations followed by sudden reversals with melting of the ice sheets – a saw-tooth pattern. The classical Snowball Earth glaciation has a different pattern with very fast build-up of ice all the way down to the equator, triggered by the albedo runaway feedback, and an as sudden melting.

The last 600 ka has been characterized by a 100 ka periodicity. In the period before 900 ka the primary cycle was ca 41 ka, paced by the orbital obliquity. The definite shift from the earlier 41 ka to a strong 100 ka cycle took place at the boundary between MIS 16 and 15 (the Termination VII) about 620 ka ago (Dean et al, 2015). The glaciations became steadily more severe over most of this period but were periodically terminated by sudden melting with climate turning back to shorter interglacials.

The caloric season insolation (leading to melting during the warm season) is the key factor for controlling ice sheets. The caloric season at lower latitudes has a 23 ka cycle (Ruddiman, 2014). On high latitudes it is the axial tilt with the 41 ka periodicity which contributes most to the solar energy input impacting mass balance of ice sheets. The ice sheet dynamics are strongly linked to ablation during warm summer season with high insolation and less by cold winter seasons. Thus, if the climate is cold enough not to start serious melting during the summer, orbital forcing will have a limited impact on ice sheet dynamics. This is i.a. the reason why the current ice age has shifted from the obliquity driven 41 ka cycle to a 100 ka cycle, when orbital forcing does not manage to trigger full deglaciation every 41 ka (Ruddiman, 2014).

The Milankovitch cycles did not have the same periods in the past. Earth's rotation rate has slowed, and the Moon is more distant today. This implies that Milankovitch cycles were shorter in the past (Berger, 2012). The precession cycle which today has a period of ca 23 ka had an estimated period of ca 19 ka at 650 Ma according to Fairchild et al (2016) or ca 15 ka according to Ruddiman (2014). In the Cryogenian, the cyclicity of the orbital obliquity was ca 25 ka (Ruddiman, 2014). Obliquity works as a driver for high latitude ice sheet fluctuations but has limited effect on low altitudes. Here precession plays a more vital role in forcing ice sheet mass balance (Benn et al, 2015).

There are different other interactions playing part in forming glacial cycles. Ice sheet development has a hysteresis in relation to the solar forcing, which can cause the ice mass balance to remain positive through several precession periods until finally the deglaciation is triggered. Other mechanisms playing a role in the glacial cycles are delay in bedrock uplift, ocean feed-back and especially CO_2 interaction (Abe-Ouchi et al, 2013). The orbital forcing is thus not the only mechanism managing the glacial cycles, which clearly show also nonlinear behaviour.

1.5 Review of proxies for climatic and environmental change

A literature review of applicable proxies has been done (Clift et al, 2014; Halverson et al, 2010; Jakobsson et al, 2000; Nesbitt and Young, 1982). There are typically four different type of proxies used when assessing climatic and environmental variations over geological time scales:

i. Indicators of chemical weathering

Typical proxies include ratios such as K/Rb and K/Al (where K is more mobile in water), C_{RAT} (chlorite versus sum of chlorite + hematite + goethite) and the Chemical Index of Alteration (CIA). CIA is a frequently used proxy for chemical weathering caused by variations in climate. Feldspar, a very common mineral in the continental crust, is susceptible to chemical weathering resulting in clay minerals. Ca, Na and K are normally removed in this process, increasing the ratio between Al and these

alkalis. Therefore, the ratio between Al-oxide (which remains after weathering) and the sum of all oxides contained in the original feldspar will give an indication about the level of chemical weathering (Halverson et al, 2010). The CIA value remains relatively stable during low grade metamorphism (Nesbitt and Young, 1982). This proxy for chemical weathering is normally written:

$$CIA = (Al_2O_3 / (Al_2O_3 + CaO + Na_2O + K_2O)) \times 100$$

A high CIA value indicates a period with warm and wet climate, while a low value indicates a colder and drier climate. In a similar fashion, a high K/Rb indicates more weathering while a high K/Al indicates less weathering.

ii. Indicators of physical erosion

Typical proxies include Ti/Ca (Ti relative to a stable pelagic biogenic Ca) indicating more erosion, clastic mass accumulation rates (MAR) indicating same, Al/Si (proportions of clay versus sand) indicating less erosion, and grain size (variations between silt and clay). These proxies typically indicate increase in fluvial or glacial mass transports, which does not necessarily need to be connected to a warmer climate. River run-off can be one such transport vehicle.

iii. Use of carbon and oxygen isotopes as indicators

$\delta^{18}O$ in benthic marine records (higher value indicating colder climate and/or more continental ice) and $\delta^{13}C$ (higher value indicating higher biological activity with warmer climate).

iv. Proxies linked to other processes

These include different proxies such as varying contents of coarser fractions (>63 µm, where interglacial/interstadials are believed to generate less coarse fractions), amount of calcareous nannofossils, Mn concentrations from riverine run-offs or oxygenation, bulk density, etc. Paleomagnetic polarity reversals are used to correlate data to a known age, which then can be used to correlate to other climate indicators.

Biostratigraphy using calcareous nannofossils is a valuable tool today when dating sediment layers. Since calcareous nannofossils did not exist in the Cryogenian, they are however not further considered in this report.

Mn is a good proxy for following glacial-interglacial sequences in the Arctic Ocean as showed by Jakobsson et al (2000) and reconfirmed by Löwemark et al (2008). Mn has a good correspondence with lower latitude $\delta^{18}O$ variations and where Mn maxima indicate warm interglacial periods with increase runoffs from large Siberian rivers. Rivers are draining peat bogs and boreal forests and are transporting the dissolved Mn to the central parts of the Arctic Ocean during active inter-glacial periods. Possibly the deep sea was also better ventilated during the inter-glacials, with oxygen causing the Mn to precipitate (Jakobsson et al, 2000). Mn has limited correlation to variations in other elements as analysed in the sediment cores. This supports the assumption that Mn has another origin (i.e. riverine) than other sediment components which may depend on other mechanisms for its variations such as transport by ice rafting (Löwemark, 2008).

Both Fe and Mn can serve as proxies for a redox environment. Anoxic sea water may contain free Fe and Mn ions which are then precipitated as oxides upon possible oxidization of the water. Anoxic conditions existed during the Snowball Earth glaciations and possibly in deep water during glacial episodes of the Arctic Ocean when ocean circulation was restricted.

Chemical weathering and physical erosion are per definition decoupled from each other but are not opposing processes and in practice show a correlation. Proxies vary either directly or indirectly with the basic climatic parameters. Since a chemical weathering proxy can be driven by temperature or precipitation (or normally by a combination of both), care should be taken to analyse drivers behind the observed change. However, weathering regimes are still considered to be closely related to climate and chemical weathering proxies are used to interpret past climatic change (Clift et al, 2014).

Repositories and time lags need to be considered. It can take tens of ka to transport erosion material from inland sources to continental margins, as estimated for the Indus basin (Clift et al, 2014). The depositional speed can be a consequence of reworking and shifting efficiency in transport modes, rather than change in the climate driven source of the proxy. Local conditions at the scene of deposition will also influence the result, such as bottom currents, slope movements etc. In summary, resolution of climate proxies is typically in the range of 10^3, which may be sufficient if studying climate variations on an orbital scale (10^4) or longer geological scales such as tectonic forcing (>10^6) (Clift et al, 2014).

Best result is expected if using a combination of proxies which produce a similar pattern.

Similar drivers of chemical weathering and erosion existed both in the Quaternary and in the Cryogenian, although some conditions were different. At times with an active hydrological cycle this was driving chemical weathering as well as erosion. However, land-based plants which contribute to chemical weathering was not present during the Cryogenian. Precipitation of Fe and Mn ions during oxygenation of anoxic sea water operated in the same way in both periods, but the extent of the ferruginous seas was different. During Quaternary and Cryogenian, erosion was more active during glacial cycles as compared to weathering. Mn serves as a good proxy for riverine run-off during the Quaternary, where Siberian rivers are draining extensive peat bogs and boreal forests during interstadials. Mn obviously did not have this type of sources during the Cryogenian and may therefore not be as useful as a riverine proxy during that time.

2. Methodology

2.1 The analyse method

Two depositional sequences have been analysed for chemical elements content: 85 cm of interglacial mudstone from the Sturtian glaciation and 722 cm of deep sea sediments from the Quaternary Period. The chemical elements content was measured with the X-ray fluorescence (XRF) method. By bombarding the sample with high energy X-rays, electrons in the constituent atoms are exited and emit characteristic secondary fluorescent radiation when falling back into their normal states. By sampling the energy states of the secondary emissions, the quantity of elements in the sample can be calculated. The method is widely used for chemical elements analysis of metals and in geochemical research.

A portable XRF analyser of type Olympus Innov-X Delta was used for the measurements. Further descriptions of the XRF method and the measurement device is available in the User Manual for the Olympus Delta™ Innov-X Analyzers (PN_103201, Rev_A: June/2010) and in Kleine et al (2016) paper.

The XRF analyser has a somewhat lower resolution (ca 1 cm diameter) and higher confidence intervals of reported data than larger stationary units normally have. Its penetration depth is ca 1 – 3 mm (Kleine et al, 2016) which can be a limiting factor if the rock surface is uneven or strongly weathered. Lighter elements and elements in lower concentrations are more difficult to detect using XRF analysers. In the actual field location, Al and P were only occasionally detected, and S and Cl data contain high

percentages of uncertainty. Si being a relatively light element also suffers from this, but since the total amount of Si in the mudstone is relatively large, uncertainty was still at an acceptable level.

Figure 9. The Olympus Innov-X Delta analyser with battery and titanium plates for calibration.

The 1 cm resolution of the XRF analyser can pose a problem when mineral crystal sizes are relatively large, where a single crystal can distort the result (Kleine et al, 2016). This is however not a major concern in the actual measurements, where the sediment core only contains very small size clasts and the mineral crystal sizes in the Islay mudstone are small. The low resolution of 1 cm also implies that annual cyclicities will not be possible to detect and a measurement accuracy in the order of 100 – 200 yrs. is more likely (subject to depositional rates). It shall also be noted that the chosen balance between accuracy and speed, resulting in measurement taken every cm, will give a resolution within the data log of ca 500 – 1000 yrs. As an example, a climate shift such as the Little Ice Age in the 16th to 19th century could have been missed.

The Olympus XRF analyser is calibrated before use with help of a titanium plate.

The absolute values of XRF element measurements are distorted by the amount of air between the detector muzzle and the sample surface. This is especially the case when a core surface is uneven, strongly weathered, cracked or when samples previously had been removed from the core (which is frequent in the Arctic Ocean sediment core). However, since the atmosphere mainly consists of light elements (N_2 and O_2), such measurement distortions lead to some increase of reported light elements (LE) but rather small % error within the actual proportions of elements followed.

Some practical observations were derived from the actual measurements. It is highly recommended to make continuous notes from the measurements, writing down the actual position (cm mark), analysers reading number and the reported value of e g LE. This enables a safe later correlation of the dataset with the measured object and allows for corrections of possible human errors such as wrong positioning of the instrument.

The reported data are uncertain both as regards random variations in the XRF sampling and analysing of data, but also because of small variations in exact positioning of the analyser. For future field measurements, it is recommended to regularly make practical assessment of the aggregated confidence interval of the data. This can e g be done by making repeated measurements on the same location of the sample. If making 20 repeated measurements at the same spot, the total variation in data for each reported element would give an estimate of a 5% confidence interval for each such element. This practical assessment of the confidence interval of the chemical elements data was unfortunately not performed in the actual two measurements.

2.2 Description of field measurements on the interglacial sequence done on Islay

The field measurement of chemical elements in the Islay mudstone sequence was done in March 2018. The interglacial mudstone sequence is located in a rock outcrop in the vicinity of Loch Lossit on Islay.

Figure 10. Rock outcrop in Loch Lossit, Islay, containing the interglacial mudstone sequence.

The part of the rock outcrop to be analysed was inspected and measured. The total length of the mudstone sequence was 85 cm. To enable exact positioning of the Olympus XRF analyser, it was marked up with a marker pen in sections of 10 cm.

Figure 11. The interglacial mudstone sequence, outlined by the white rectangle.

In field conditions measurements are more easily distorted. NaCl in sea spray can travel far in stormy conditions which may distort Cl readings. Because of this, and since measurement uncertainty is higher in lighter elements, Cl has not been utilized in the geochemical analysis. Detected amounts of both Cl as well as Al have therefore been added to LE in the analysis of the field data.

The studied interglacial mudstone sequence is located above the Great Breccia but below the Disrupted Beds. Just above the mudstone layer, a thin (ca 50 cm) sandstone sequence is conformingly placed. Below the mudstone and above the sandstone, layers of dolostone can be seen.

Figure 12. Rock types in the studied sequence of the Port Askaig Formation. A: Dolostone located on top of the sequence, B: Dolostone located in bottom of the sequence, C: Dropstone observed within the mudstone, D: The analysed mudstone, E: Sandstone located just above the mudstone.

2.3 Description of lab measurements on Arctic Ocean sediment core

The lab measurement of the Arctic Ocean sediment core was done in March and April 2018 in the SLAM lab in Stockholm University. The sediment core is one of 24 piston cores acquired during the 1996 Arctic Ocean expedition on the icebreaker Oden and is identified as AO96/12-1pc (i.e. the 12th core collected during the 1996 Arctic Ocean expedition, being a piston core). The core consists of horizontally bedded silty clay and clay. The length of the core is 722 cm. The upper 15 – 20 cm upper part of the AO96/12-1pc core was not recovered (Jakobsson et al, 2000).

AO96/12-1pc was acquired from the Lomonosov ridge close the North Pole at a depth of 1003 mbsl, at 144°46’22’’E, 87°05’51’’N (Jakobsson et al, 2001). Seismoacoustics sonar sounding has indicated a major erosion caused by ice-berg or grounded ice down to a level of ca 1000 mbsl on the Lomonosov ridge. The area where the 96/12-1pc was retrieved was not affected by the erosion. (Jakobsson et al, 2001).

The sediment core was recovered with help of the Stockholm University piston/gravity coring system. The system has the capacity to acquire up to 12 m long sediment cores and is operated from the aft deck of IB Oden (Bolin Center, 2016).

Six-meter-long transparent polycarbonate liners, which then are cut into 150 cm section, are used to store the cores. The AO96/12-1pc is contained in 5 such cylinders. After recovery, the core is split along its length into an archive and working half. These halves are marked with the core number, type (archive respectively working half), and section length. The cylinder is marked along its side with depth in cm (Jakobsson et al, 2007).

Upon recovery, AO96/12-1pc was analysed regarding density (GRAPE) variations, p-wave velocity and magnetic susceptibility at 1-cm intervals. Fraction >μ63 mm was counted and content of different calcareous nannofossil was noted. Colour variations was analysed with help of an image capturing system (Jakobsson et al, 2000; Jakobsson et al, 2001). Major and trace elements were determined for 121 samples using ion coupled plasma atomic emission spectroscopy, ICP-AES (Walsh, 1997 cited in Jakobsson, 2000).

The chemical elements content of the AO96/12-1pc has been analysed several times. The initial ICP-AES measurement is considered the most reliable. The Mn concentration were also measured using a stationary XRF scanner of type TATSCAN-F2 (O'Regan et al, 2008). Löwemark et al (2008) used an Itrax X-ray fluorescence scanner (Stockholm University stationary Itrax core scanner) to analyse the archive half of the AO96/12-1pc core. The Itrax XRF scanner used a 5 mm interval, while the portable Olympus XRF has a wider scanning width of 10 mm. The Itrax XRF use a 10 s exposure versus a longer 35 s used in the portable Olympus XRF. Because of this short detection times and scattering in dataset, the Itrax dataset is considered as semi-quantitative.

This new measurement with the Olympus XRF analyser was done on the archive half, except for section cm 240 – 275 which was missing. Measurement of this section was done on the working half. It was noted that this section of the archive half is also missing from the dataset collected during the Itrax scanning in 2008.

Care is always taken to prevent the core from being exposed for longer period, to avoid further drying out. Regardless of this, numerous cracks were observed in the archive half which made measurements difficult in those areas.

General difference in results can be expected from using various positions along the diameter of the core. The centre part of the core has been removed in some sections of both the archive and working halves.

Figure 13. Archive half showing large cracks because of drying of sediments.

2.4 Data handling

The data log retrieved from the Olympus XRF analyser has been matched to the cm positions on the respective mudstone sequence and sediment core. To obtain a continuous dataset, a few manual adjustments were done where measurement was not possible (i.e. because of cracks in the sediment core). Here data were interpolated from the closest upper and lower locations.

All elements followed in this study have been normalized to their respective average value. Thus, variations in element concentration throughout the length of the core are seen as percentage shifts around their average values. An alternative to normalize the elements to LE has been considered but was discarded. The assumption is that when measurement contains more atmospheric elements (N,

O) then the reported weight % of other elements would be proportionally lower and that a normalization would thus reduce random scattering in the data. However, LE concentration shows also a variation over time because of varying content of lighter elements (e g Al, Cl and Na in the Port Askaig mudstone) and of "organic" elements such as O, C, N, and H included in minerals. If to normalize with LE, such trends would distort the pattern of elements followed. A few tests were done which confirm this to be the case and which showed no visible reduction in data scattering.

When utilizing LE (light elements) in the analysis, intermittently detected elements have been added to LE in order to show a consistent composition of this parameter. This means that LE for the Port Askaig mudstone includes Al, Cl and some other minor elements, while the AO96/12-1pc includes Cl and some minor elements.

An analysis of correlation of data has been done. These include correlation between different elements within each dataset (the Port Askaig mudstone, respectively the AO96/12-1pc) to understand which elements follow and depend on each other. Correlation of the new Olympus XRF data versus data from earlier measurements of the AO96/12-1pc has also been done, which gives some better understanding of the usability and accuracy of the Olympus XRF analyser. Conclusions from these analyses are presented in the Result section.

In the graphical presentation of data, each individual value is shown as a point. A moving average has also been added to the graphs to help identify underlaying trends. For the longer series of the AO96/12-1pc core, a moving average of 10 cm was judged to provide a suitable trade-off between random scattering and trend visibility. For the shorter series of the Port Askaig mudstone, a moving average of 5 cm was selected. As a comparison, a moving average of 3 cm was used when analysing the Itrax XRF data for the LOMROG cores (Hanslik et al, 2013), and 5 cm in Sellén et al's (2010) analysis of sediment cores.

The following proxies from the XRF measurements of chemical elements were considered in this study:

- For Cryogenian climate change recorded in the Port Askaig mudstone sequence: K/Rb (weathering), Ti/Ca (erosion), Fe (redox environment), Mn (redox environment)
- For Quaternary climate change recorded in the Arctic Ocean sediment core: K/Rb (weathering), K/Al (weathering), Ti/Ca (erosion), Al/Si (erosion), Mn (riverine), Fe (redox environment)

3. Results

3.1 Reliability of data

Average confidence intervals as reported in output data from the XRF analysers are shown in Table 1. This statistical data shall however only be understood as indicative, and actual uncertainty in the dataset may also be influenced by other factors such as human operator errors. A limiting factor when using proxies in this study has been uncertainty in XRF measurements of lighter elements. Al which is a vital component in several of the proxies, is not always detected in the field measurement of the Islay mudstone. Al has a quite large confidence interval in the laboratory measurements of the Arctic Ocean sediment core.

	element	LE	Al	Si	S	Cl	K	Ca	Ti	V	Cr	Mn	Fe	Cu	Zn	As	Rb	Sr	Y	Zr	Pb
PAF mudstone	average wt%	61,71	9,04	17,57	0,231	0,418	2,849	1,917	0,362	0,030	0,012	0,106	12,58	0,026	0,010	0,002	0,014	0,014	0,003	0,014	0,007
	average conf. interval	0,78	2,18	0,66	0,036	0,086	0,058	0,034	0,024	0,009	0,004	0,007	0,22	0,002	0,001	0,001	0,001	0,001	0,000	0,001	0,001
	conf. interval %	1,3%	24,2%	3,8%	15,8%	20,7%	2,0%	1,8%	6,8%	29,1%	32,0%	6,3%	1,7%	7,1%	10,6%	29,5%	4,3%	3,9%	15,0%	4,4%	12,6%
AO96/12 core	average wt%	61,49	7,38	21,21	0,112	2,813	1,897	0,472	0,364	0,031	0,012	0,124	4,20	0,003	0,007	0,002	0,009	0,012	0,002	0,014	0,002
	average conf. interval	1,12	1,53	0,64	0,026	0,135	0,043	0,015	0,022	0,008	0,003	0,006	0,08	0,001	0,001	0,000	0,000	0,000	0,000	0,000	0,000
	conf. interval %	1,8%	20,8%	3,0%	23,0%	4,8%	2,3%	3,1%	6,1%	25,9%	29,4%	5,0%	2,0%	25,7%	9,1%	17,9%	4,3%	3,4%	13,3%	3,4%	23,9%

Table 1. Average confidence intervals of XRF measured element weights.

The quality of the acquired data has been ascertained by controlling correlation with other datasets available for the Arctic Ocean sediment core. Correlation between Mn and Fe in the Olympus XRF measurement of the AO96/12-1pc versus other earlier measurements of same elements in this core shows a good consistency between Olympus XRF and ICP-AES data, but less so concerning Itrax XRF data. It shall be noted that the Itrax analyser primarily provide qualitative results with lower precision and that it does not correlate very well with the ICP-AES measurements. Conclusion from these comparisons gives that the Olympus XRF provides more reliable results than the stationary Itrax analyser.

Fe_2O_3 (ICP-AES)	1,000		
Fe Itrax	0,764	1,000	
Fe Olympus	0,855	0,767	1,000
	Fe_2O_3(ICP-AES)	Fe Itrax	Fe Olympus

MnO (ICP-AES)	1,000		
Mn Itrax	0,574	1,000	
Mn Olympus	0,792	0,455	1,000
	MnO (ICP-AES)	Mn Itrax	Mn Olympus

Table 4. Cross-correlation between different Fe and Mn measurements of the AO96/12-1pc.

Correlation coefficients have also been calculated between Olympus XRF measured elements and physical properties registered for the AO96/12-1pc. They show generally little covariance with those physical properties. Only Si correlate with p>0.5 with density (GRAPE) and acoustic impedance, and Fe, Zn and Rb negatively (p>-0.5) with P-wave with corrected velocity. None correlate with susceptibility and shear vane. Since the use of these physical properties as proxies for climate change lies outside of the scope of this study, this has not been investigated further.

3.2 Internal correlation between elements in each dataset

The analysis of correlation between different elements is summarized in the tables below. Shades of red indicate strength of positive correlations while shades of blue indicate strength of negative correlations. Mn shows clear positive correlation with Si, K and Fe in the Port Askaig mudstone, but no significant correlation with other elements in the AO96/12-1pc data. The lack of correlation of Mn with other elements in the Arctic Ocean sediments has been noted before (Löwemark et al, 2008). Correlation between LE and other elements is primarily interpreted to originate from uncertainties in detection method, where not detected elements are added to LE. The lightest elements and such elements that only exist in low concentrations thus show the strongest negative correlation.

LE	1,00													
Si	-0,96	1,00												
S	0,29	-0,20	1,00											
K	-0,84	0,93	-0,10	1,00										
Ca	0,54	-0,70	-0,31	-0,77	1,00									
Ti	-0,81	0,85	-0,19	0,89	-0,59	1,00								
Mn	-0,67	0,67	-0,18	0,63	-0,60	0,53	1,00							
Fe	-0,63	0,60	0,17	0,52	-0,71	0,44	0,63	1,00						
Zn	0,34	-0,26	0,37	-0,24	-0,10	-0,25	-0,22	0,00	1,00					
Rb	-0,29	0,38	-0,10	0,55	-0,30	0,63	0,09	-0,02	-0,08	1,00				
Sr	-0,63	0,63	-0,37	0,65	-0,37	0,49	0,63	0,30	-0,40	0,02	1,00			
Y	-0,06	0,07	-0,03	0,04	-0,06	0,07	0,11	0,04	0,34	-0,03	0,08	1,00		
Zr	-0,15	0,12	-0,02	0,16	0,03	0,33	-0,17	-0,01	0,07	0,62	-0,25	0,06	1,00	
Pb	0,65	-0,39	-0,14	-0,21	0,00	-0,30	-0,23	-0,36	0,25	0,07	-0,23	-0,10	-0,27	1,00
	LE	Si	S	K	Ca	Ti	Mn	Fe	Zn	Rb	Sr	Y	Zr	Pb

Table 2. Correlation coefficients (r) between measured chemical elements in Port Askaig mudstone. LE is inclusive of Al and Cl when detected.

Löwemark et al (2008) noted some correlation in the dataset generated by their Itrax scanning of the AO96/12-1pc, which included Si vs. Al, K and Ti, Cl vs. Sr and Zr, K vs. Rb and Sr vs. Ti. As can be seen in the table below, the Si vs. Al and the two Cl vs. Sr and Zr correlations are not repeated in this dataset. In view of the shorter detection cycle of the Itrax analyser and the amount of scattering in the lighter elements derived therefrom, these correlations reported by Löwemark (2008) are now believed to have been random.

LE	1,00													
Al	-0,68	1,00												
Si	-0,76	0,13	1,00											
Cl	0,37	-0,31	-0,33	1,00										
K	-0,63	0,31	0,52	-0,69	1,00									
Ca	-0,19	-0,04	0,17	0,06	0,13	1,00								
Ti	-0,41	0,04	0,53	-0,09	0,18	0,08	1,00							
Mn	0,01	0,03	-0,12	-0,15	0,18	-0,08	-0,14	1,00						
Fe	-0,09	0,32	-0,32	-0,43	0,44	-0,08	-0,22	0,20	1,00					
Zn	-0,18	0,27	-0,09	-0,58	0,59	-0,08	-0,05	0,23	0,77	1,00				
Rb	-0,35	0,29	0,16	-0,73	0,84	-0,04	0,03	0,24	0,68	0,78	1,00			
Sr	-0,23	-0,15	0,48	0,20	0,05	0,23	0,48	-0,05	-0,55	-0,41	-0,19	1,00		
Y	-0,21	0,13	0,15	-0,40	0,46	-0,03	0,13	0,11	0,35	0,42	0,47	0,04	1,00	
Zr	-0,24	-0,15	0,55	0,15	-0,07	0,06	0,55	-0,18	-0,63	-0,47	-0,28	0,66	-0,01	1,00
	LE	Al	Si	Cl	K	Ca	Ti	Mn	Fe	Zn	Rb	Sr	Y	Zr

Table 3. Correlation coefficients (r) between measured chemical elements in AO96/12-1pc.

3.3 Port Askaig interglacial mudstone data

The main chemical elements of the Port Askaig mudstone are presented below. Position along the mudstone sequence is shown on the x-axis with 0 at the bottom and 85 at the top of the rock section. Elements where XRF analysis provide unreliable data have been excluded. This is typically lighter

elements and elements in small concentrations which are not detected in every XRF probe. Below elements which include Si, K, Ca, Ti, Mn, Fe and Rb display less scattering and have more constrained patterns. The graphs include a moving average of 5 cm to enable identification of data-trends.

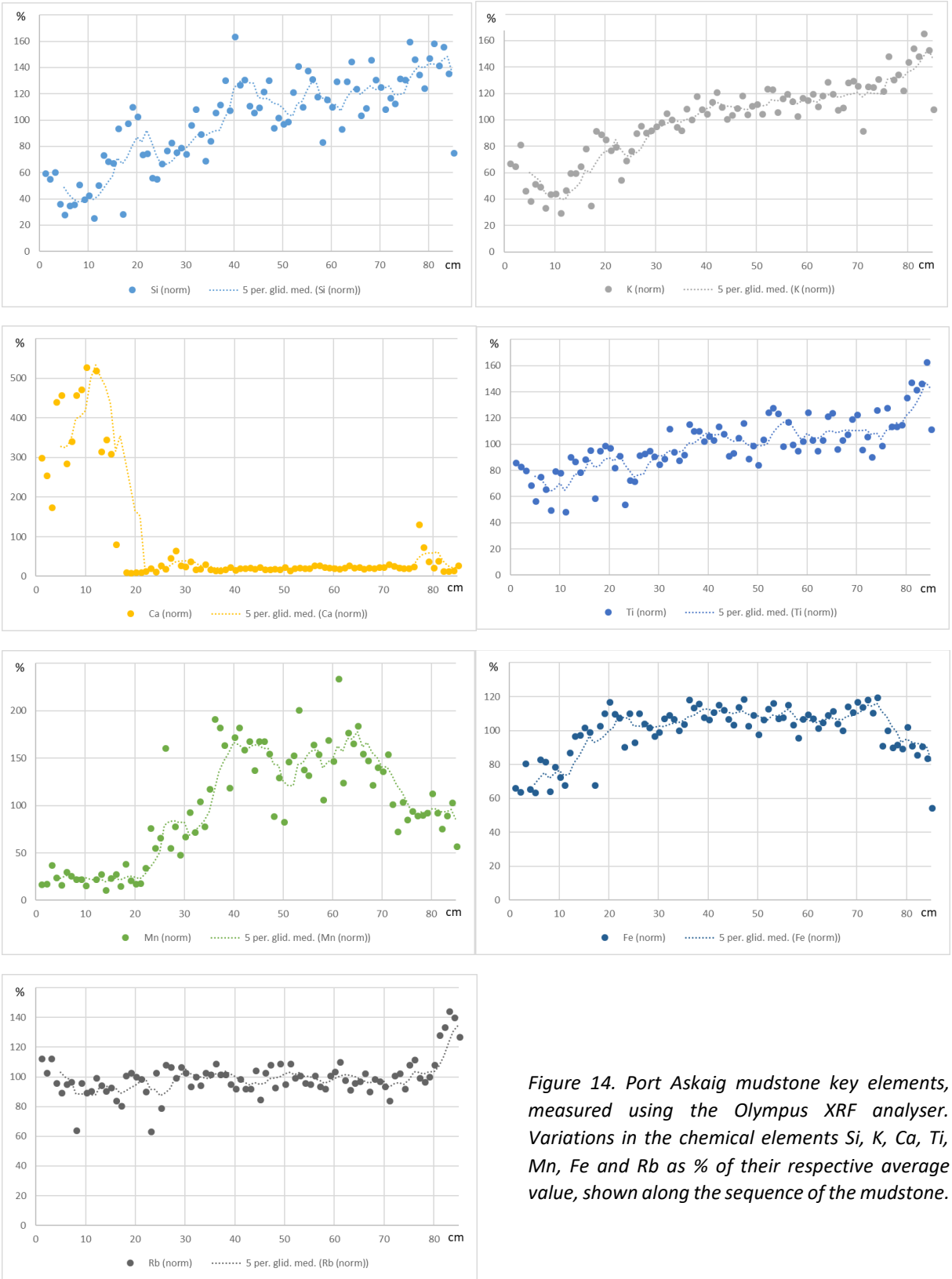

Figure 14. Port Askaig mudstone key elements, measured using the Olympus XRF analyser. Variations in the chemical elements Si, K, Ca, Ti, Mn, Fe and Rb as % of their respective average value, shown along the sequence of the mudstone.

Si and K concentrations show positive growths of ca 3 times over the length of the sample. Ca has a large excursion in the first 18 cm of the sample, after which it settles at a steady lower value. Ti shows a moderate growth of ca 2 times. Both Mn and Fe show similar pattern with an initial increase followed by a high plateau and a decline in the last 10 – 15 cm. Rb is stable until the last 5 cm when it jumps ca 50%.

The initial Ca excursion is shown below with the XRF data aligned to the mudstone. A fraction of the rock has been eroded in this lower part of the mudstone outcrop, which leaves this surface ca 10 cm below the surface of the rest of the mudstone.

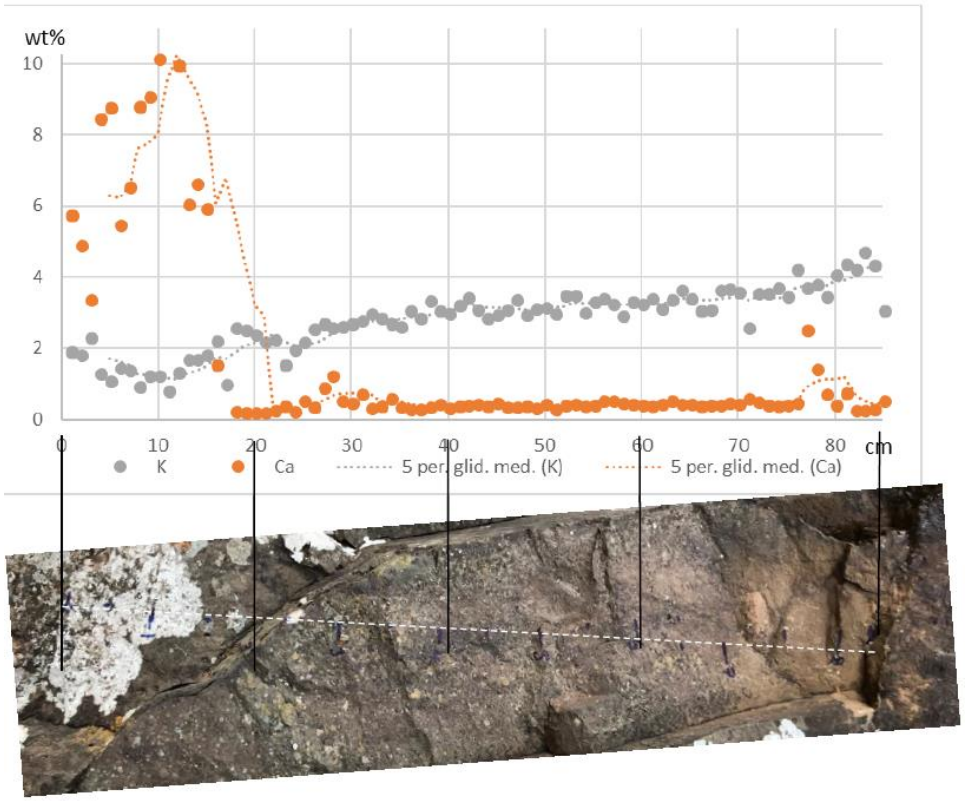

Figure 15. Graph showing Ca values correlated with line indicating positions of measurements in the mudstone sequence. The observed Ca anomaly is within the bottom ca 18 cm, where a block of the rock is removed.

Data for the following proxies representing Cryogenian climate change are presented in the graph below: Ti/Ca as indicator of erosion, K/Rb as indicator of weathering and Fe and Mn as indicators of a redox environment. Data have been normalised to respectively averages and the trends are shown as moving averages of 5 cm.

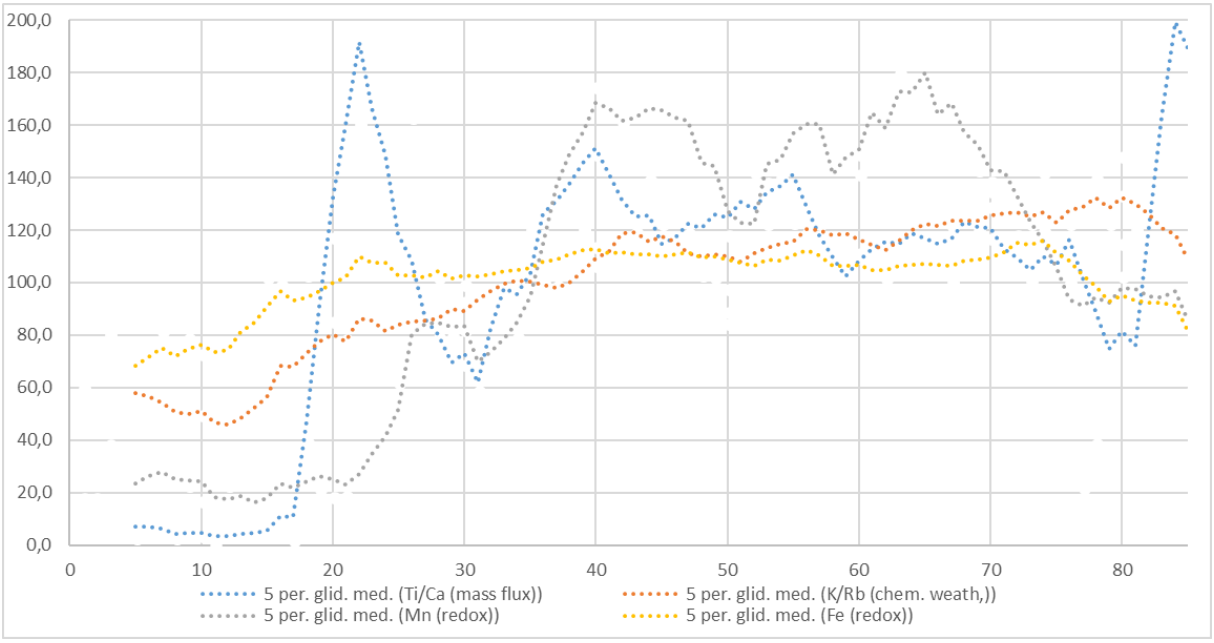

Figure 16. Cryogenian climate proxies as represented by chemical elements in the Port Askaig mudstone sequence.

The reliability of proxies is considered higher when several of them show a similar pattern. The above proxies have been evaluated based on their correlation, with the result listed the table below.

correlation coefficients	
Ti/Ca vs K/Rb	0,498
Ti/Ca vs Mn	0,297
Ti/Ca vs Fe	0,578
K/Rb vs Mn	0,654
K/Rb vs Fe	0,653
Mn vs Fe	0,631

Table 5. Correlation coefficients of Cryogenian climate proxies from Port Askaig Formation.

The relative proportions of the main chemical components vary over the length of the rock sample, i.e. over time. This is shown in Figure 18. with the weight % displayed of Fe, Mn, Ca, Si plus all other elements summed in LE (those being primarily O, Al, Cl, S and some trace elements in smaller amounts).

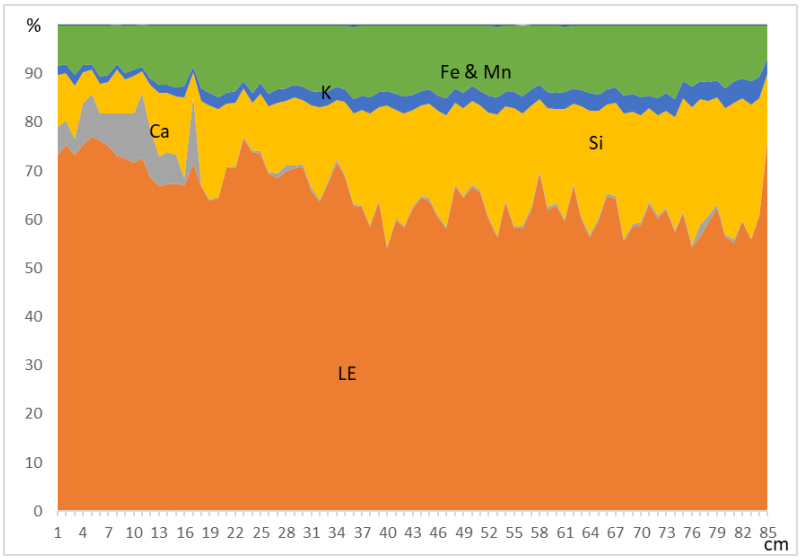

Figure 17. Variation in relative concentrations of Fe, Mn, K Si, Ca and Light Elements along the Port Askaig mudstone sequence

3.4 AO96/12-1pc data

The dataset containing the measurements of chemical elements in the AO96/12-1pc display some specific features compared to the Port Askaig mudstone. Since it covers a more than 8 times longer distance (722 cm as compared to 85 cm), more variations appear in the data possibly indicating cyclic changes. The conditions under which the measurement was done (a lab instead of field environment and a flat even surface allowing better alignment of the measuring nozzle) also generate less

uncertainty in the data output. For example, the AO96/12-1pc dataset contain a continuous range of Al values, which mostly were not detected in the Port Askaig mudstone.

The figure below shows cyclicity of certain key elements (Al, Si, K, Ca, Ti, Mn, Fe, Rb, LE) in AO96/12-1pc, which will serve as a base for later comparison with Port Askaig data in the discussion section. Graphs below include a moving average of 10 cm to enable identification of data-trends. As can be seen from the graphs, the lighter elements. Al shows more scattering than heavier elements such as e.g. Fe.

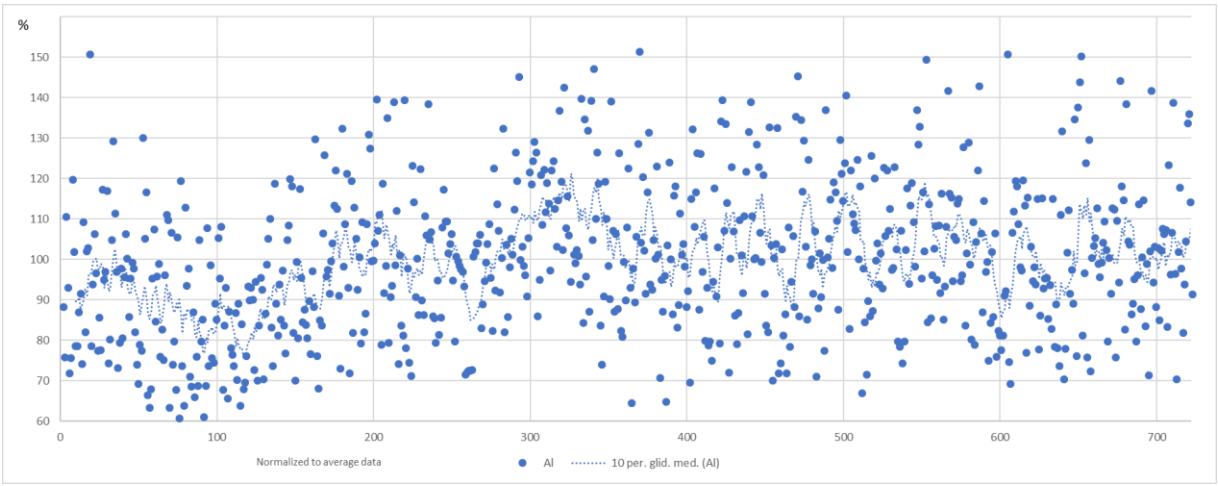

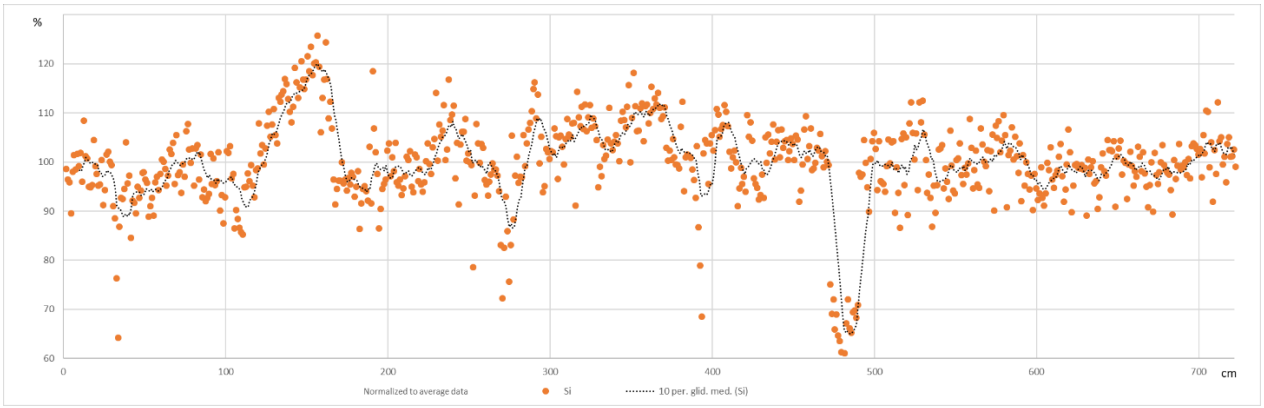

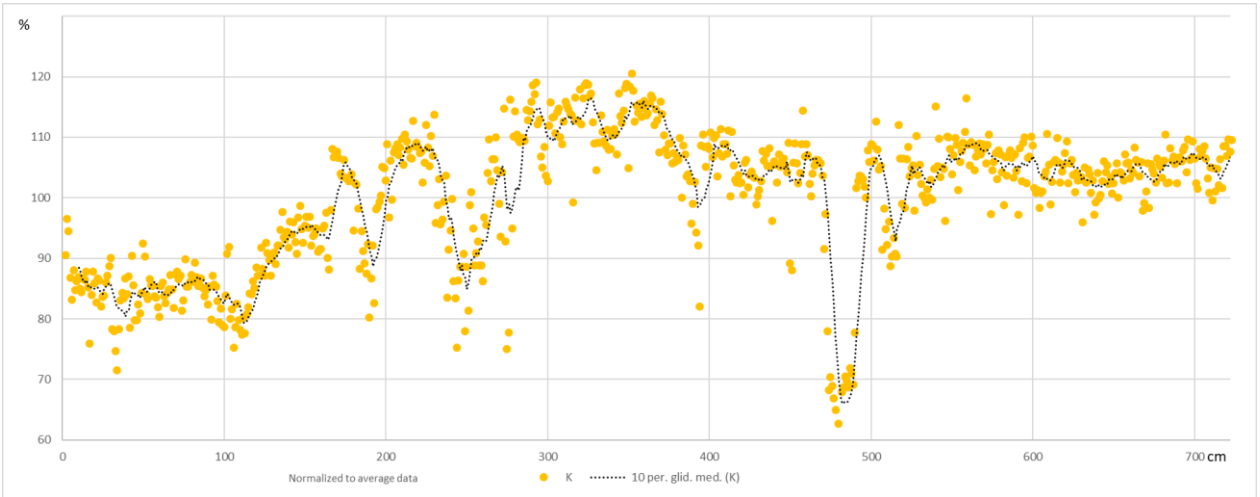

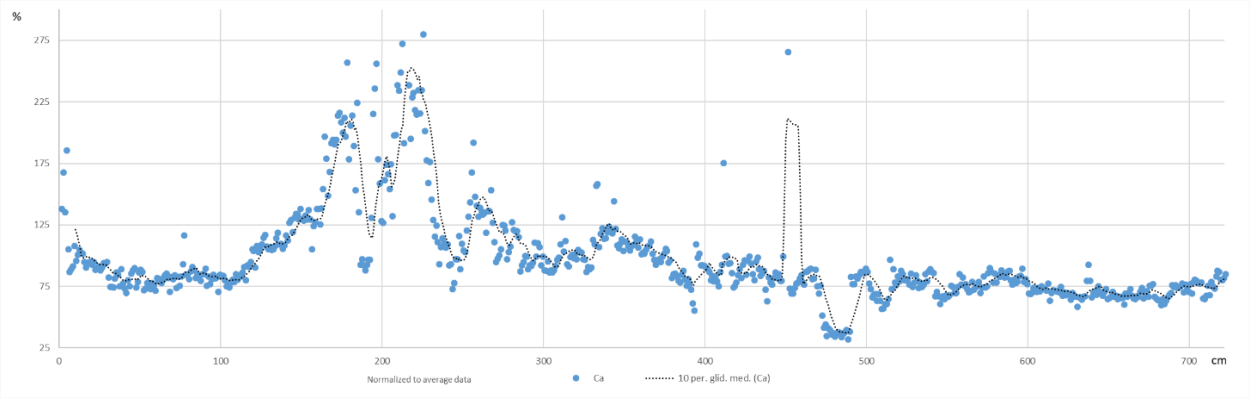
%
275
225
175
125
75
25
0
100
200
300
400
500
600
700
cm
Normalized to average data
Ca
10 per. glid. med. (Ca)

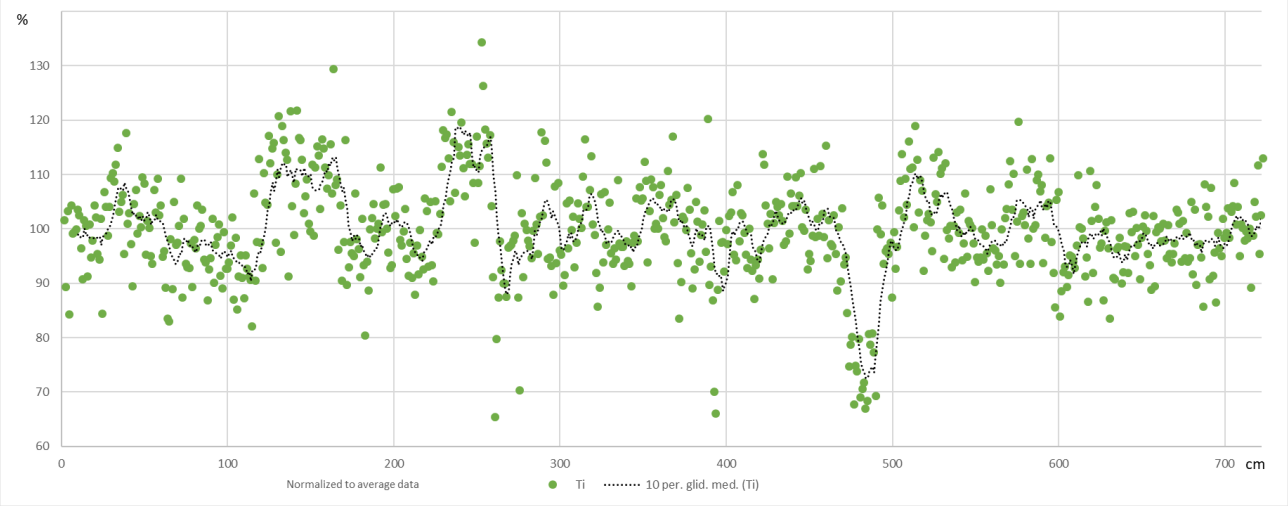
%
130
120
110
100
90
80
70
60
0
100
200
300
400
500
600
700
cm
Normalized to average data
Ti
10 per. glid. med. (Ti)

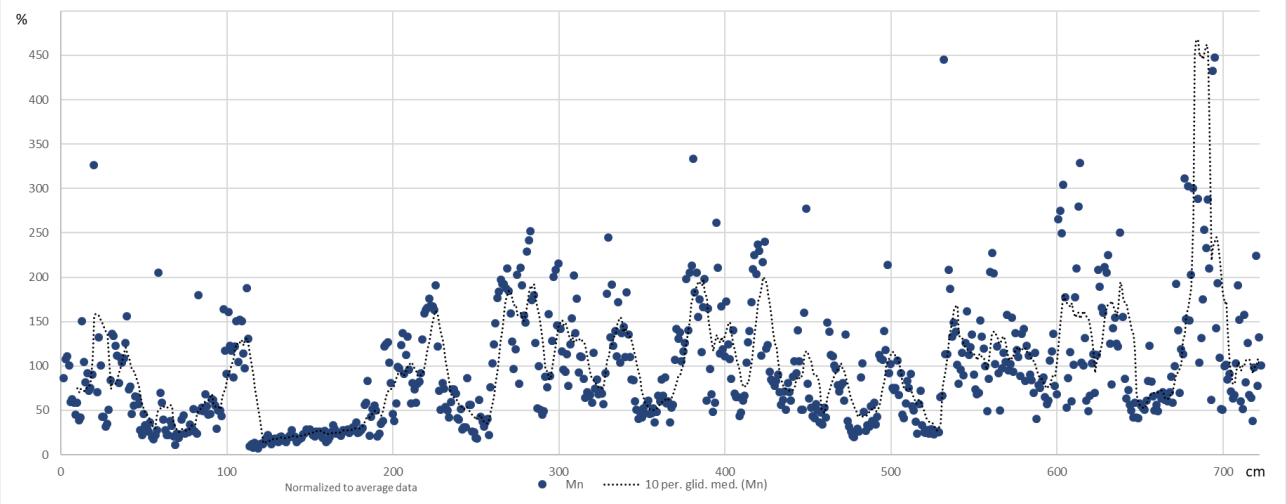
%
450
400
350
300
250
200
150
100
50
0
0
100
200
300
400
500
600
700
cm
Normalized to average data
Mn
10 per. glid. med. (Mn)

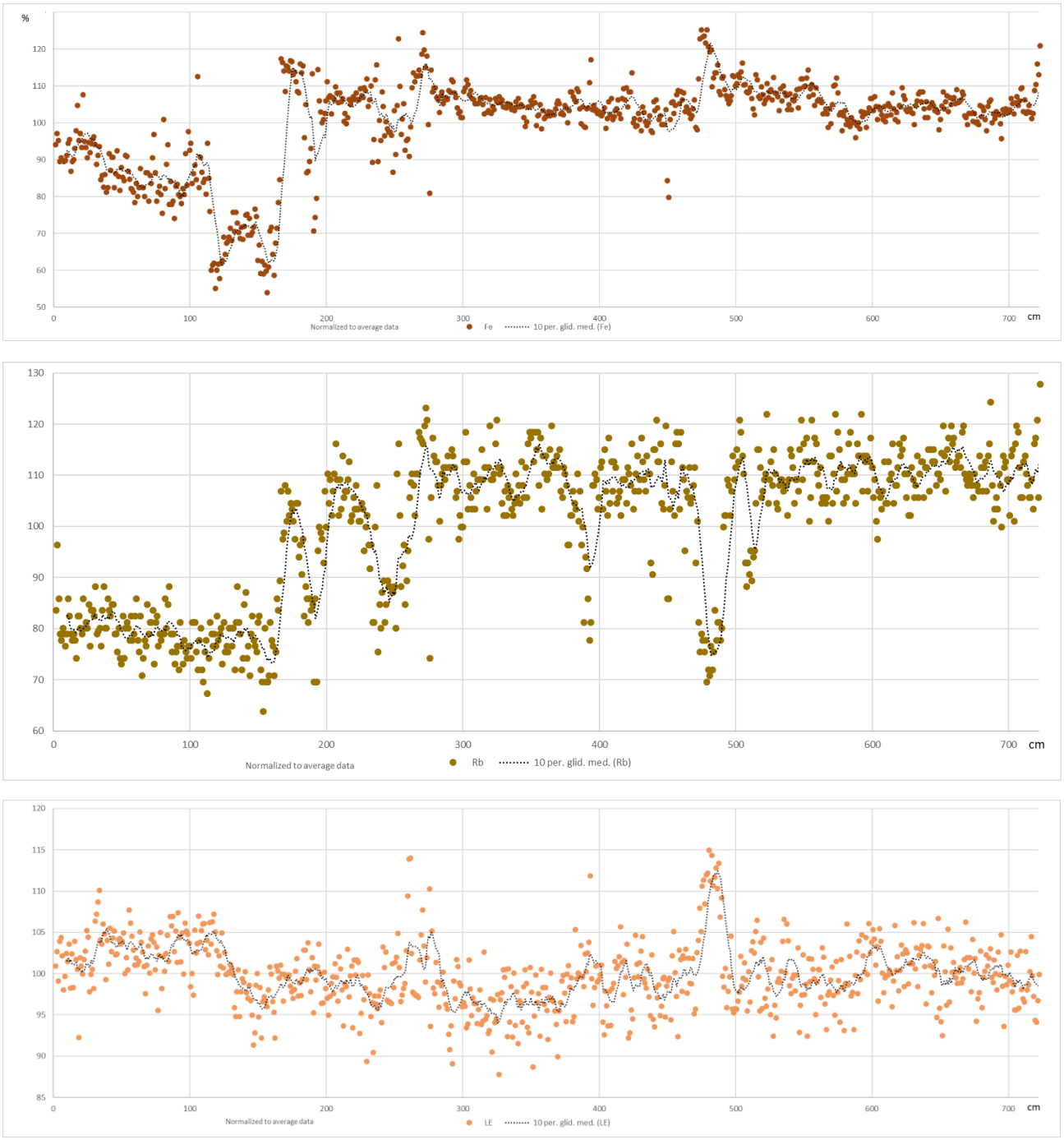

Figure 18. AO96/12-1pc key elements, measured using the Olympus XRF analyser. Variations in the chemical elements Al, Si, K, Ca, Ti, Mn, Fe, Rb and LE as % of their respective average value, shown along the sequence of the sediment core.

Certain elements show similar variation patterns. Si varies in tandem with K and Ti as do Rb with Fe and K. Some co-variance between K, Al and Si would be expected to be generated by clastic sediments containing feldspar. As earlier noted, Mn does not generally show similarities with other elements.

The most pronounced fluctuations are seen in Mn, Fe, Rb, Ca and K with pronounced peaks or throughs more than 25% from their respective average value. Especially Mn shows such very pronounced variations. Löwemark et al (2008) reported strong variations in Fe, Ti, K and Si.

A very pronounced anomaly is seen in certain elements between the depth 472 – 489 cm. The Si, K, Ca, Ti and Rb show sharp decreases and Fe increases. It shall be noted that Fe and Ti otherwise seem to vary in tandem. Also, of interest is the sharp increase of the measurement of light elements which primarily includes organic elements.

Data for the following proxies representing Quaternary climate change are presented in the graph below: Ti/Ca and Al/Si as indicators of erosion, K/Rb and K/Al as indicators of weathering, Mn as indicator of riverine run-off and ocean circulation and Fe as indicator of a redox environment. Data have been normalised to respectively averages and the trends are shown as moving averages of 10 cm.

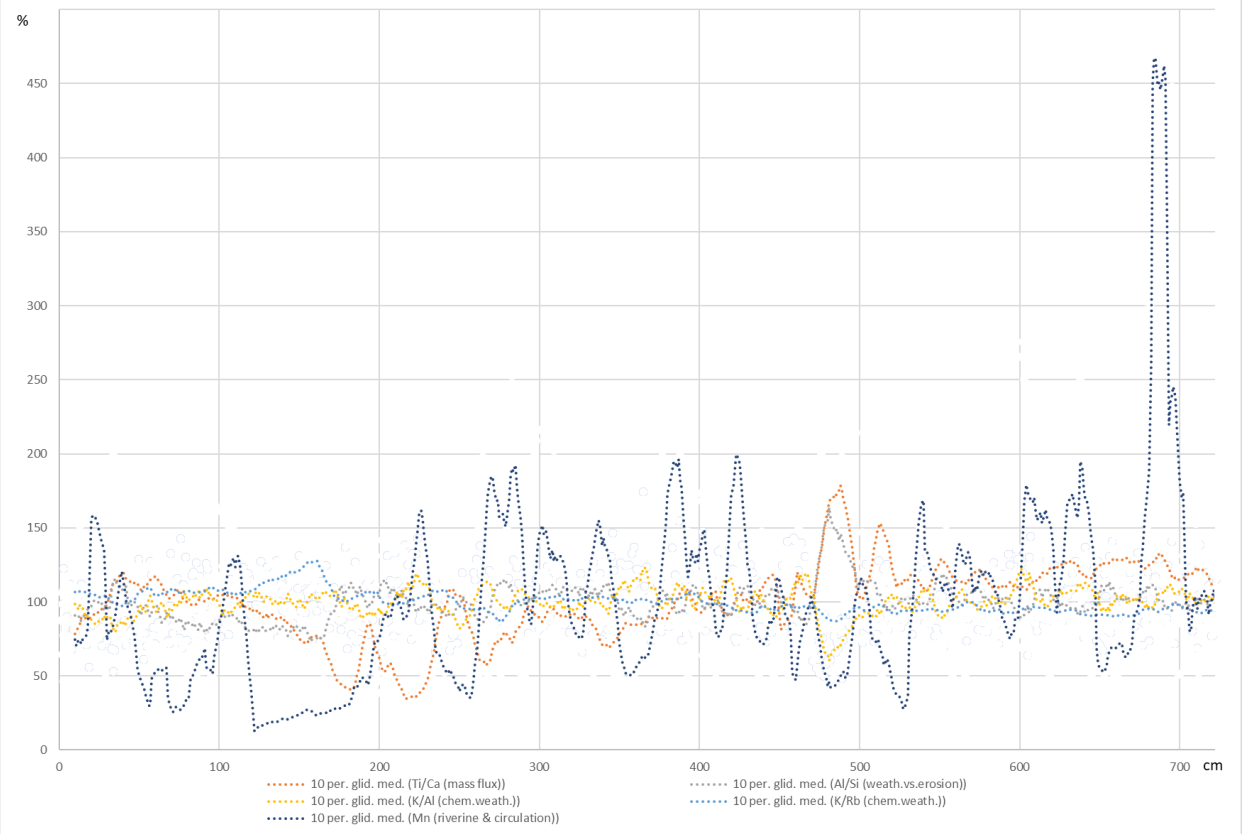

Figure 19. Quaternary climate proxies as represented by chemical elements in AO96/12-1pc.

correlation coefficients	
K/Al vs Ti/Ca	-0,214
K/Al vs Al/Si	-0,839
K/Al vs K/Rb	0,014
K/Al vs Mn	0,075
Ti/Ca vs Al/Si	0,252
Ti/Ca vs K/Rb	-0,368
Ti/Ca vs Mn	0,055
Al/Si vs K/Rb	-0,310
Al/Si vs Mn	0,058
K/Rb vs Mn	-0,193

Analysis of correlation coefficients between these various proxies is presented in the table to the left. The highest (negative) correlation is found between K/Al versus Al/Si, but which is likely driven by the inclusion of Al in both ratios (as numerator respectively denominator). The data otherwise show little evidence of covariance, and a common background factor such as e g climate is thus not evident.

Table 6. Correlation coefficients of Quaternary climate proxies from AO96/12-1pc.

4. Discussion

4.1 Interpretation of proxy data and discussion about possible orbital driven cycles

The Sturtian glaciations are generally expected to be severe and therefore more comparable to the more recent 100 ka regime within the Quaternary period. The transition between the 41 ka cycles which dominated from ca 2.75 Ma and the present 100 ka cycles is happening gradually between 600 ka and 900 ka (Ruddiman, 2014), and the change within the 100-ka regime from low to higher amplitude glaciation-interglaciation cycles is at MIS 6, i.e. at ca 191 ka (Jakobsson et al, 2001). This would imply that comparison with the full length of the AO96/12 core is relevant. A qualitative analysis of chemical elements-based proxies from the AO96/12-1pc however give limited correlation between their periodicity and that of the number of MIS periods or the number of $\delta^{18}O$ peaks in this period. In this analysis only strong trend-shifts are recorded to avoid random fluctuations to be interpreted as a signal. This is achieved by only noting a new peak or through when the 10 cm moving average trendline has cut a longer 50 cm trendline which act as a constraint.

section:	0-100 cm		100-200 cm		200-300 cm		300-400 cm		400-500 cm		500-600 cm		600-700 cm		700-722 cm		sum 0-722 cm	
max/min:	UP	DOWN	UP	DOWN	UP	DOWN	UP	DOWN	UP	DOWN	UP	DOWN	UP	DOWN	UP	DOWN	UP	DOWN
K/Rb (weathering)	4	2	2	2	2	2	3	3	4	4	4	5	3	2	1	2	**23**	**22**
K/Al (Weathering)	3	2	4	4	3	2	4	5	4	4	5	4	4	4	2	3	**29**	**28**
Ti/Ca (erosion)	1	2	2	1	3	3	1	2	5	5	3	3	3	3	1	1	**19**	**20**
Al/Si (erosion)	2	3	4	3	3	3	6	6	4	4	2	3	4	4	2	1	**27**	**27**
Mn (riverine)	1	1	1	1	2	2	3	2	3	4	3	3	3	2	0	1	**16**	**16**
Fe (redox environ.)	1	1	3	3	2	1	0	1	2	1	1	2	0	0	0	0	**9**	**9**
Number of MIS periods according to Jakobsson et al (2000) age model covering full MIS 1 - 28:																		
	2	1	1	1	2	2	2	2	2	2	2	2	2	3	1	1	**14**	**14**
Number of MIS including MIS sub-stages (Mn matched to δ18O peaks, indicating warm maximum), according to Jakobsson et al (2000):																		
	2		2		6		5		5		3		3				**26**	

Table 7. Numbers of possible glacial-interglacial cycles for each 100 cm section of the AO96/12-1pc are estimated from the variations in proxies in AO96/12-1pc. For comparison the number of full MIS periods from Jakobsson et al (2000) age correlation of the core is included, as well as the number of $\delta^{18}O$ maximums (Jakobsson et al, 2000).

The chemistry of the deep-sea waters of the Arctic Ocean and the Cryogenian oceans where the Port Askaig tillite was formed was different, with a relatively well oxygenated bottom at least during Quaternary interglacials versus a continuous anoxic ferruginous deep sea with very low sulphate content at that time (Hood and Wallace, 2014; Hoffman et al, 2017).

The fact that Mn shows correlation with other elements in the Port Askaig mudstone and broadly follows Fe indicates that it is not a proxy of the same type seen in the Arctic Ocean. Fe and Mn show only minor correlation in the AO96/12-1pc data, which limits the comparability between these two sets when using Fe and Mn as proxies for a redox environment.

A possible explanation for the de-coupling of Mn from other elements in the Arctic Ocean is the difference in transport processes. Most elements found in the sediment are delivered by ice rafting, while Mn is delivered in dissolved form through large runoffs from Siberian rivers during warmer periods and precipitated as MnO because of varying ventilation of Arctic Ocean deep waters (Jakobsson et al, 2000; Löwemark et al, 2008). The covariance between Mn and Fe in the AO96/12-1pc dataset is likely to have been larger if both elements had been supplied in an equivalent way.

The driver for the variation in Mn in the Port Askaig mudstone is the same mechanism as interpreted for Fe, i.e. precipitation of MnO in a redox environment. Mn is furthermore interpreted as being included in the Fe-oxide as a contamination.

A qualitative analysis of chemical elements-based proxies from the Port Askaig mudstone section possibly give one main cycle throughout the length of the sample. K/Rb representing weathering shows

a gradual increase of weathering over the length of the section, while Fe and Mn representing oxygenation in a redox environment both show higher levels in the middle part of the section. Ti/Ca representing erosion has the most variable pattern with possibly four peaks indicating more erosion. These observations are together interpreted as representing one interglacial cycle, as will be shown in the discussion regarding the paleoclimatic and paleoenvironmental setting for the Port Askaig interglacial section.

Benn et al (2015) and Fairchild et al (2016) have found indications in Svalbard of a possible Milankovitch orbital forcing in late stage of a Snowball Earth glaciation. Although Milankovitch precession cycle can have played a role in the late stage of a Snowball Earth glaciation when CO_2 had built up to sufficiently high levels, it is not evident that it will be visible in the Port Askaig Formation provided that its age is constrained to the early 10 Ma part of the Sturtian glaciation as Ali et al (2017) indicate. Furthermore, since present Milankovitch orbital forcing of glaciations is far from straightforward and require help from coupled non-linear mechanisms such as change in atmospheric and ocean circulation (which require a better understanding of paleogeography), it is difficult to predict how a Neoproterozoic orbital forcing would operate, if at all.

Since the Port Askaig Formation was deposited in a subtropical paleogeography, the type of Milankovitch cycle to have an impact (if any) would be the precession. Obliquity (tilt) plays a limited role at low latitudes. It shall also be noted that precession at Cryogenian had a period of ca 15 – 19 ka (Ruddiman, 2014) as compared with the current periodicity of ca 23 ka. In addition to Milankovitch orbital solar forcing, there are numerous other factors which may have an impact on the possible length and amplitude of a Cryogenian glacial cycle. These include for example a more precise location and composition of the paleocontinents which in their turn would have impact on ocean deep water currents and atmospheric circulation.

Assuming that the Port Askaig mudstone sequence was laid down during the shorter interglacial phase of one full Milankovitch 15 – 19 ka precession cycle, a deposition rate of ca 10 – 15 cm / ka would have been required. This may be possible in a coastal-near marine environment but is far above the sedimentation rates of the Arctic Ocean e g as shown in the AO96/12-1pc. In conclusion, it is difficult to ascertain if the Milankovitch precession cycles played any role during the deposition of the studied sequence of the Port Askaig mudstone.

4.2 A paleoclimatic and paleoenvironmental interpretation of the Port Askaig interglacial section

The Arctic Ocean's sedimentation regime during the Quaternary is well described in the literature with transport mechanisms and sedimentation rates based on a constrained age model. Based on similarities between the Arctic Ocean's processes and the Port Askaig Tillite interglacial mudstone sequence, certain assumptions can be made as to the paleoenvironment in Islay including range of sedimentation rates, deposition environment and transport mechanisms.

Most of glacial sediments transported by ice ends up on continental shelves. Since shallow marine sediments have good chances of being preserved, it is natural that this is the type of glaciogenic depositional paleoenvironment that is found today (Eyles, 1988). Fairchild et al (2016) infers a sedimentation rate in their Cryogenian interglacial Svalbard sequence of 2.8 cm/ka which seem to be well in line with e g AO96/12-1pc data (Jakobsson et al, 2001).

The primary mechanism for transporting sediments into the central Arctic Ocean is ice rafting. The lowest sedimentation rates are found in areas with permanent sea ice, where it is likely to be in mm/ka or even lower. Therefore, neither the sediment in the AO96/12-1pc nor the Port Askaig mudstone would have been deposited under permanent sea ice.

The observed dropstone in the studied mudstone sequence which overlies the Great Breccia indicates that iceberg or ice shelf were present during the time when the mudstone was deposited. In conclusion, the Port Askaig mudstone is proposed to have been deposited on a marine continental shelf with a sedimentation rate in the range of cm per ka. Depositional mechanism would involve ice rafting (i.e. from an ice shelf or from icebergs).

Precipitated iron-oxide found in Sturtian banded iron formations is primarily hematite (Fe2O3). This is typically joined by jasper (SiO2). Classical Snowball Earth hypothesis explained these iron rich deposits associated with the Sturtian glaciation as being a terminal event when Earth shifted from the icehouse to greenhouse stage with opening oceans being oxygenated. The Sturtian iron formation was formed at redoxclines in the water column where anoxic Fe-rich water met with well oxygenated surface or fresh water of meteoric origin. This would have placed the banded iron formation at a similar stratigraphic level as the cap carbonate, but which evidently is not the case everywhere. The analysed interglacial mudstone is located rather early between the Great Breccia and the Disrupted Beds. The interpreted stratigraphy of the studied interglacial sequence of the Port Askaig Formation is presented in the figure below.

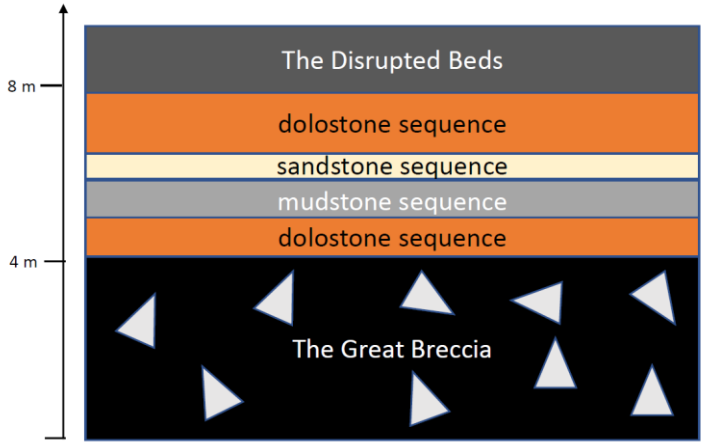

Figure 20. Stratigraphy of the interglacial mudstone sequence. Approximate thickness of respective layer is indicated by the vertical scale, based on Ali et al (2017) and field observations.

Its iron-oxide content of ca 15 wt% and fine grained sedimentary structure qualifies it as an ironstone (Hoffman et al, 2017), which clearly indicates an oxygenated deposition environment, and which contradicts the classical Snowball Earth Hypothesis. Similarly located ironstones are also observed in other glacial sediment sequences from the Cryogenian, e g in the Adelaide Rift Complex in Southern Australia (Le Heron et al, 2011).

There are indications of an anoxic and very ferruginous ocean also after the end of the Sturtian glaciation at ca 650 Ma (Hood and Wallace, 2014). Also, Fairchild et al (2016) make similar observations in a sequence of rock in Svalbard originating from the warm period between the Sturtian and Marinoan glaciations. The water column below a peritidal chemocline contained an abundance of iron(II) and only coastal waters were oxygenated by wave actions or oxidized fresh water. Although there is no direct explanation for the occurrence of free iron in an open ocean at that time, it would (if held true) lead to certain implications. Extreme climatic variations and global glaciations of a Snowball Earth could not have been the sole reason for a ferruginous deep ocean condition which lasted at least 10 Ma after the end of the Sturtian glaciation (Hood and Wallace, 2014). The occurrence of ferric oxide in the studied mudstone from the Port Askaig Formation need to be deposited in a shallow (peritidal) environment, and also the source material for the Disrupted Beds needs to have a similar origin.

In conclusion, the varying wt% proportion of Fe in the analysis could be driven by transgression/regression events instead of a final oxygenation after melting of an ice cover.

Furthermore, assuming that the source of Fe (II) was from an anoxic ocean and considering the lateral extent of the Disrupted Beds, the depositional setting has likely been marine instead of lacustrine. If Eyles (1988) and Ali et al (2017) interpretations of sandstone layers in the Port Askaig Formation as forming in a tidally influenced environment are correct, it would rule out a lacustrine environment since tidal action would require a direct connection to a larger ocean. A marine environment is thus supported by this evidence of a tidal environment, and furthermore the absence of seasonal layers normally associated with a lacustrine setting.

There are several observations indicating that most of the diamictite layers in the Port Askaig Formation really have a glacial origin and not being subaqueous flows of turbidite type as proposed by Eyles (1988). These observations include i.a. dropstones, indicating ice rafted material. The lateral extent of the diamictite layers also contradicts a turbidite interpretation. The erosional surfaces which are seen in the Arctic Ocean and in the sea surrounding the Antarctica are caused by grounded ice, either as extended ice shelves or grounded icebergs. Since these erosional surfaces are absent in the Port Askaig diamictite horizons, it contradicts the assumption of grounded ice as a glaciogenic transport mechanism.

As described in the geological history of Islay, the Port Askaig Formation underwent a greenschist facies metamorphose during the Caledonian orogeny. This metamorphose was rather light and left much of the original minerals intact. The clay minerals in the original mudstone have been metamorphosed into muscovite. Based on the simplifying assumption that the studied section of Port Askaig mudstone only would contain quartz, limestone, muscovite and Fe- and Mn-oxides, a qualitative model of the mineral composition has been worked out. This is based on the wt% of chemical elements, including the amount of Al. Since measurement of Al has a high uncertainty and is not detected at every cm-mark, the model shall be taken as indicative only. The wt% of K, Ca, Fe and Mn have constrained the mole proportions of muscovite, calcite, hematite and manganese oxide. The mole proportions of quartz have been “toggled” to reach a full utilization of Al plus K, Ca, Fe and Mn. The resulting wt% of the minerals are displayed in the table below.

mineral	formula	cm	15	20	33	37	42	53	65	74	80	83
muscovite	$KAl_2(AlSi_3O_{10})(FOH)_2$		20,8%	27,2%	32,1%	32,1%	38,6%	39,3%	38,2%	41,7%	45,9%	49,1%
clay minerals	$Al_2Si_2O_5(OH)_4$		18,5%	9,0%	10,5%	10,3%	11,2%	15,8%	18,6%	9,0%	12,5%	0,0%
quartz	SiO_2		27,5%	42,0%	37,0%	36,1%	28,1%	22,5%	21,6%	26,5%	21,8%	33,7%
calcite	$CaCO_3$		14,9%	0,6%	1,0%	0,8%	1,1%	1,1%	1,2%	1,1%	1,1%	0,7%
hematite	Fe_2O_3		18,4%	21,1%	19,3%	20,5%	20,8%	21,0%	20,1%	21,6%	18,5%	16,4%
manganese oxide	MnO		0,0%	0,0%	0,1%	0,3%	0,2%	0,3%	0,3%	0,1%	0,2%	0,1%

Table 9. Qualitative model of mineral proportions within the Port Askaig mudstone.

Since Al is not detected at every location, the result is only calculated for 10 separate sections along the mudstone sequence. The result is shown in the figure below. Some less intuitive conclusions can be drawn from the figure below showing the changing mineral composition. Si is increasing along the length of the mudstone section, but since K is increasing even more this lead to a reduction in quartz while muscovite is increasing.

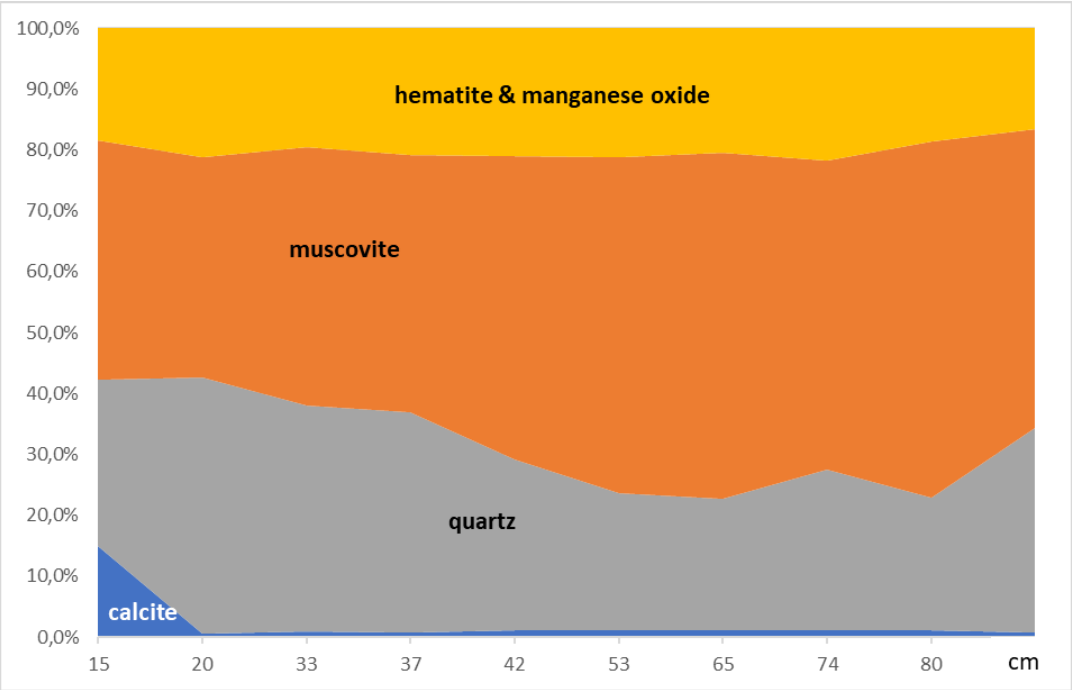

Figure 21. Qualitative view of how key constituent minerals in the mudstone change over time.

Based on the literature review, results from the XRF data logs and interpretations made in this discussion section, the paleoclimatic and environmental setting for the Port Askaig mudstone section is summarized as follows:

- The mudstone sequence shows one climatic and environment event in a shallow marine setting.
- An interglaciation period starts with sudden warming causing the cover of sea ice to melt, resulting in precipitation of calcium as witnessed by the dolostone layer below the studied mudstone sequence.
- The precipitation of calcium continues in the early part of the mudstone deposition, until depleted.
- Continental ice sheets start to melt, with calving of icebergs and ice rafting of glaciogenic materials being deposited into a shallow marine continental shelf.
- Melting of continental ice sheets cause an isostatic rebound with lowered sea level and which places the sea bottom within a peritidal environment.
- Wave action in the peritidal zone oxygenate upper parts of the water column, which cause Fe (II) and dissolved Mn to oxidize and precipitate as hematite (with Mn as contamination in the hematite).
- Warmer climate increase chemical weathering as evidenced by increasing content of muscovite higher up in the mudstone sequence.
- The isostatic rebound is eventually raising the depositional surface above the sea level, when the precipitation of Mn and Fe-oxide drops off.
- Wave-action deposit the sand forming the sandstone layer which sits on top of the studied mudstone sequence.

A summary of arguments supporting and contradicting the interpretation of the depositional environment (marine versus lacustrine), glaciogenic transport mechanisms (ice-rafting versus grounded ice) and the control mechanism of the diamictite horizons of the Port Askaig Formation are presented in the tables below. As indicated in the discussion below, the author of this paper supports the conclusions that the Port Askaig Formation was formed by climate controlled (although unclear if

by a hard Snowball Earth or Slushball Earth model), deposited in a marine environment by ice rafting of glaciogenic material.

climatic controlled	tectonic controlled	ice rafting	grounded ice
lateral extent contradicts a mega-turbidite	shifting height of the Great Breccia	similarities with AO96/12-1pc	the Great Breccia being tectonite
observations of dropstones		no erosional surfaces	
changing clast types		dropstones	

marine depositional setting	lacustrine depositional setting
ferruginous ocean source for observed high Fe oxide content	a constant depositional depth would indicates absence of global sea level change
lateral extent of different horizons would require a very large lake	
tidal depositional environment require direct access to large ocean	
seasonality of a lacustrine deposit is not evident	

Table 10. Summary of observations supporting and opposing certain open questions concerning the paleoenvironment conditions controlling the deposition of the Port Askaig Formation.

There are certain interpretations that can be made from observations in this paper that are both supporting and contradicting the Snowball Earth hypothesis. These are summarized in the table below. Not surprisingly, they do not provide a clear conclusion as to the validity of this hypothesis.

Snowball Earth with one cycle driven by albedo & CO2	Several glacial-interglacial cycles driven by other processes
tillite deposited by grounded ice	variable depositional mechanisms including ice rafting
cap carbonates being formed at the end of the ice age	indications of open seas
$\delta_{13}C$ excursions caused by collapsing biosphere	glacial and interglacial rock sequences
a ferrous ocean with BIF formed at end of the ice age	ironstones early in stratigraphic sequence

Table 8. Interpretations of observations which both supports and contradicts the Snowball Earth hypothesis.

4.3 Interpretation of other observations

Jakobsson et al (2001) and O'Regan (2008) noted a unique pink sediment layer in the AO96/12-1pc core at 471 – 488 cm depth, which also correspond to a low-density excursion (less coarse wt% >63µm). Löwemark et al (2008) noted excursions in measured Fe, Ti, K and Si at the same depth. No hypothesis as to its origin has been put forward in these papers.

The same anomaly is clearly seen in the new Olympus XRF log from the AO96/12-1pc. Certain elements between the depth 472 – 489 cm show a very pronounced excursion. The Si, K, Ca, Ti and Rb show sharp decreases and Fe increases. It shall be noted that Fe and Ti otherwise seem to vary in tandem. Of interest is also the sharp increase of the measurement of light elements which primarily includes organic elements. The anomaly is summarized in the table below.

	deviation (%)		range (cm)		average	uncertainty	
element	pos.	neg.	start	stop	weight (%)	weight (%)	comment
LE	12,5%		471	489	61,49%	1,8%	possibly incl. S, P
Si		30%	472	489	21,21%	3,0%	
Cl	20%		472	489	2,81%	4,8%	also possible anomaly at 392-393 cm
K		30%	472	489	1,90%	2,3%	
Mn					0,12%	5,0%	no clear anomaly
Ca		60%	472	489	0,47%	3,1%	
Fe	25%		472	481	4,20%	2,0%	
Zn					0,007%	9,1%	no clear anomaly
Ti		25%	473	489	0,36%	6,1%	
Rb		25%	472	489	0,086%	4,3%	
Sr		60%	472	489	0,012%	3,4%	
Zr		50%	472	489	0,014%	3,4%	

Table 11. Anomaly observed in the AO96/12-1pc

The positive excursion of LE likely indicate an increase of lighter organic elements, including organic carbon. This would typically accumulate in an anoxic environment. The negative excursions of several elements would thus indicate more limited proportions of clastic elements. This anomaly is located at ca 630 ka and roughly coincides with the sudden warming at the border between MIS 15 and 16. The author posits that this anomaly was caused by a wave of abundant nutrients from increased weathering combined with solar energy at the MIS16/15 boundary leading to an extreme blooming of phyto-planktons. The anomaly seen is the accumulation of organic elements (especially carbon) in an anoxic environment at bottom of the sea. Similar observations from the MIS 16/15 boundary has been observed in the Santa Barbara basing (Dean et al, 2015). Since the same pink colour and density anomaly is also seen in other sediment cores from the Arctic Ocean (O'Regan et al, 2008), it could possibly serve as a common dated marker when synchronizing chronology of these cores.

5. Conclusion

The studied interglacial mudstone sequence from the Port Askaig Formation is interpreted as being deposited in a shallow marine setting at semitropical latitudes during an episode of global warming in the early part of the Sturtian glaciation. The transport mechanism of glaciogenic material was primarily by ice rafting. The high content of hematite is an indication of oxygenation in a peritidal zone when isostatic rebound caused a sea level regression. Increasing amounts of muscovite higher up in the mudstone indicates increased weathering. The underlaying sequence of dolostone and overlaying sequence of sandstone are consistent with this paleoclimatic and paleoenvironmental interpretation. One interglacial phase is thus observed, which possibly could be attributed to Milankovitch orbital forcing.

The interpretation of the paleoclimatic setting of studied interglacial mudstone sequence from the Port Askaig Formation does not give support for the Snowball Earth hypothesis in its "hard" version. Other observations as noted in the introduction summary of literature reviews do not either support this hypothesis. This include observations of glacial-interglacial cycles, short duration of glacial episodes within the cycle, evidence of open seas, the existence of a ferruginous sea also before the start of the Sturtian glaciation and BIF found not only at the end of the ice age. Different energy-balance models allowing for steady state solutions with open waterbelts at low latitudes are however needed to support a Slushball Earth alternative.

Some further work is recommended to be undertaken in relation to the Port Askaig Formation. A more comprehensive documentation of the content and variation of Fe oxide in both interglacial sequences as well as within the matrix of the diamictite horizons would possibly tell us something more of the depositional environment, including transgression and regression of the sea level during the time the Port Askaig Formation was built up.

The comparisons between the portable Olympus XRF data and geochemical (ICP-AES) analysis made on the AO96/12-1pc indicate a relatively good consistency. The portable XRF generally produce less scattered and better correlated data than the stationary Itrax core scanner. It is thus recommended to include the portable Olympus XRF detector in future Arctic Ocean expeditions as one of the analysing tools to be used on the working half after having recovered the piston- and gravity sediment cores.

6. Acknowledgements

This thesis is made as a part of the Bachelor's Programme in Earth Science, Distance Learning, provided by the Department of Geological Sciences. The author would like to thank prof. Alasdair Skelton not only for excellent support as supervisor for this thesis project, but also for being an inspirational and engaging teacher of geology and setting the example for what scientific work is all about. The generous support given by prof. Martin Jakobsson providing access to the sediment core from the AO96 expedition and extensive help by Carina Johansson in handling the AO96/12-1pc archive halves and guidance in the SLAM Lab is fully recognized.

The author also wishes to convey his sincere appreciation to Stockholm University for providing the distance learning programme in geology, which offers the opportunity to engage in and learn a subject of great interest. The field excursions in Scotland with inspirational teaching also gave the opportunity to meet and befriend a likeminded set of international students.

7. References

Abe-Ouchi, A., Saito, F., Kawamura, K., Raymo, M. E., Okuno, J., Takahashi, K. & Blatter, H., 2013, Insolation-driven 100,000-year glacial cycles and hysteresis of ice sheet volume: Nature, v. 500, p. 190 – 194.

Ali, D. O., Spencer, A. M., Fairchild, I. J., Chew, K. J., Anderton, R., Levell, B. K., Hambrey, M. J., Dove, D. & Le Heron, D. P., 2017, Indicators of relative completeness of the glacial record of Port Askaig Formation, Garvellach Islands, Scotland: Precambrian Research (available online 5 December 2017), p. 1 – 14.

Arnaud, E. & Eyles, C. H., 2002, Catastrophic mass failure of a Neoproterozoic glacially influenced continental margin, the Great Breccia, Port Askaig Formation, Scotland: Sedimentary Geology, v. 151, p. 313 – 333.

Arnaud, E. & Eyles, C. H., 2006, Neoproterozoic environmental change recorded in the Port Askaig Formation, Scotland: Climatic vs tectonic controls: Sedimentary Geology, v. 183, p. 99 – 124.

Benn, D. I. & Prave, A. R., 2006, Subglacial and proglacial glaciotectonic deformation in the Neoproterozoic Port Askaig Formation, Scotland: Geomorphology, v. 75, p. 266 – 280.

Benn, D. I., Le Hir, G., Bao, H., Donnadieu, Y., Dumas, C., Fleming, E. J., Hambrey, M. J., McMillan, E. A., Petronis, M. S., Ramstein, G., Stevenson, C. T. E., Wynn, P. M. & Fairchild, I. J., 2015, Orbitally forced ice sheet fluctuations during the Marinoan Snowball Earth glaciation: Nature Geoscience, v. 8, p. 704 – 708.

Berger, A., 2012, A brief history of the astronomical theories of paleoclimates, *in* Berger, A. eds., Climate Change, p. 107 – 129, Springer-Verlag, Wienna.

Bolin Center for Climate Research, 2016, Cruise Report SWERUS-C3 LEG 2: SU-AB, Stockholm, 190 p.

Clark, P. U., Dyke, A. S., Shakun, J. D., Carlson, A. E., Clark, J., Wohlfarth, B., Mitrovica, J. X., Hostetler, S. W. & McCabe, A. M., 2009, The Last Glacial Maximum: Science, v. 325, p. 710 – 714.

Clift, P. D., Wan, S. & Blusztajn, J., 2014, Reconstructing chemical weathering, physical erosion and monsoon intensity since 25 Ma in the northern South China Sea: A review of competing proxies: Earth-Science Reviews, v. 130, p. 86 – 102.

Cohen, K. M., Finney, S. C., Gibbard, P. L. & Fan, J.-X., 2017, International Chronostratigraphic Chart: International Commission on Stratigraphy, v. 2017/02, www.stratigraphy.org.

Dean, W. E., Kennett, J. P., Behl, R. J., Nicholson, C. & Sorlien, C. C., 2015, Abrupt termination of Marine Isotope Stage 16 (Termination VII) at 631.5 ka in Santa Barbara Basin, California: Paleoceanography, v. 30, p. 1373–1390,

Donnadieu, Y. & Ramstein, G., 2002, Is high obliquity a plausible cause for Neoproterozoic glaciations?: Geophysical Research Letters, v. 29, no. 23, p. 42-1 – 42-4.

Dunbar, G. B., Naish, T. R., Barret, P. J., Fielding, C. R. & Powell, R. D., 2008, Constraining the amplitude of late Oligocene bathymetric changes in Western Ross Sea during orbitally-induced oscillations in the East Antarctica Ice Sheet: (1) Implications for glacimarine sequence stratigraphic models: Palaeogeography, Palaeoclimatology, Palaeoecology, v. 260, p. 50 – 65.

Eyles, C. H., 1988, Glacially- and tidally-influenced shallow marine sedimentation of the late Precambrian Port Askaig Formation, Scotland: Palaeogeography, Palaeoclimatology, Palaeoecology, v. 68, p. 1 – 25.

Fairchild, I. J. & Kennedy, M. J., 2007, Neoproterozoic glaciation in the Earth System: Journal of the Geological Society, v. 164, p. 895 – 921.

Fairchild, I. J., Bonnand, P., Davies, T., Fleming, E. J., Grassineau, N., Halverson, G. P., Hambrey, M. J., McMillan, E. M., McKay, E., Parkinson, I. J. & Stevenson, C. T. E., 2016, The late Cryogenian warm interval, NE Svalbard: Chemostratigraphy and genesis: Precambrian Research, v. 281, p. 128 – 154.

Fairchild, I. J., Spencer, A. M., Ali, D. O., Anderson, R. P., Anderton, R., Boomer, I., Dove, D., Evans, J. D., Hambrey, M. J., Howe, J., Sawaki, Y., Shields, G. A., Skelton, A., Tucker, M. E., Wang, Z. & Zhou, Y., 2017, Tonian-Cryogenian boundary sections of Argyll, Scotland: Precambrian Research (available online 20 September 2017), p. 1 – 28.

Halverson, G. P., Wade, B. P., Hurtgen, M. T. & Barovich, K. M., 2010, Neoproterozoic chemostratigraphy: Precambrian Research, v. 182, p. 337 – 350.

Hanslik, D., Löwemark, L. & Jakobsson, M., 2013, Biogenic and detritral-rich intervals in central Arctic Ocean cores identified using x-ray fluorescence scanning: Polar Research, v. 32, p. 1 – 10.

Hoffman, P. F., Kaufman, A. J., Halverson, G. P. & Schrag, D. P., 1998, A neoproterozoic Snowball Earth: Science, vol. 281, p. 1342 – 1346.

Hoffman, P. F., Halverson, G. P., Domack, E. W., Maloof, A. C., Swanson-Hysell, N. l. & Cox, G. M., 2012, Cryogenian glaciations on the southern tropical paleomargin of Laurentia (NE Svalbard and East

Greenland), and a primary origin for the upper Russøya (Islay) carbon isotope excursion, v. 206-207, p. 137 – 158.

Hoffman, P. F., Abbot, D. S., Ashkenazy, Y., Benn, D. I., Brocks, J. J., Cohen, P. A., Cox, G. M., Creveling, J. R., Donnadieu, Y., Erwin, D. H., Fairchild, I. J., Ferreira, D., Goodman, J. C., Halverson., G. P., Jansen, M. F., Le Hir, G., Love, G. D., Macdonald, F. A., Maloof, A. C., Partin, C. A., Ramstein, G., Rose, B. E. J., Rose, C. V., Sadler, P. M., Tziperman, E., Voigt, A. & Warren, S. G., 2017, Snowball Earth climate dynamics and Cryogenian geology-geobiology: Science Advances, v. 3, p. 1 – 43.

Hood, A. V. S. & Wallace, M. W., 2014, Marine cements reveal the structure of an anoxic, ferruginous Neoproterozoic ocean: Journal of the Geological Society, v. 171, p. 741 – 744.

Hurtgen, M. T., Arthur, M. A., Suits, N. S. & Kaufman, A. J., 2002, The sulfur isotopic composition of Neoproterozoic seawater sulfate: implications for a snowball Earth: Earth and Planetary Science Letters, v. 203, p. 413 – 429.

IPCC, 2014, Climate Change 2014: Synthesis Report, Contribution of Working Groups I, II and III to the Fifth Assessment Report of the Intergovernmental Panel on Climate Change, R.K. Pachauri and L.A. Meyer (eds.), IPCC, Geneva, Switzerland, 151 p.

Jakobsson, M., Lövlie, R., Al-Hanbali, H., Arnold, E., Backman, J. & Mörth, M., 2000, Manganese and color cycles in Arctic Ocean sediments constrain Pleistocene chronology: Geology, v. 28, p. 23 – 26.

Jakobsson, M., Lövlie, R., Arnold, E. M., Backman, J., Ployak, L., Knutsen, J.-O. & Musatov, E., 2001, Pleistocene stratigraphy and paleoenvironmental variation from Lomonosov Ridge sediments, central Arctic Ocean: Global and Planetary Change, v. 31, p. 1 – 22.

Jakobsson, M., 2002, Hypsometry and volume of the Arctic Ocean and its constituent seas: Geochemistry, Geophysics, Geosystems, v. 3, no. 5, p. 1 – 18.

Jakobsson, M., Backman, J., Murray, A. & Lövlie, R., 2003, Optically Stimulated Luminescence dating supports central Arctic Ocean cm-scale sedimentation rates: Geochemistry, Geophysics, Geosystems (G^3), v. 4, no. 2, p. 1 – 11.

Jakobsson, M., Marcussen, C. & LOMROG Scientific Party, 2008, Lomonosov Ridge off Greenland 2007 (LOMROG) Cruise Report: Special Publication Geological Survey of Denmark and Greenland, Copenhagen, 122 p.

Jakobsson, M., Nilsson, J., O'Regan, M., Backman, J., Löwemark, L., Dowdeswell, J. A., Mayer, L., Ployak, L., Colleoni, F., Anderson, L. G., Björk, G., Darby, D., Eriksson, B., Hanslik, D., Hell, B., Marcussen, C., Sellén, E. & Wallin, Å., 2010, An Arctic Ocean ice shelf during MIS 6 constrained by new geophysical and geological data: Quaternary Science Reviews, v. 29, p. 3505 – 3517.

Jakobsson, M., Andreassen, K., Bjarnadottir, L. R., Dove, D., Dowdeswell, J. A., England, J. H., Funder, S., Hogan, K., Ingolfsson, O., Jennings, A., Larsen, N. K., Kirchner, N., Landvik, J. Y., Mayer, L., Mikkelsen, N., Möller, P., Niessen., F., Nilsson, J., O'Regan, M., Polyak, L., Nörgaard-Pedersen, N. & Stein, R., 2014, Arctic Ocean glacial history: Quaternary Science Reviews, v. 92, p. 40 – 67.

Jakobsson, M., Backman, J., O'Regan, M., Stranne, C., Barrientos Macho, N., Coxall, H., Eriksson, B., Flodén, T., Johansson, C., Mohammad, R., Nilsson, J., Gustafsson, Ö., Noormets, R., Anderson, L., Björk, G., Cronin, T., Gemery, L., Kirchner, N., Koshurnikov, A., Ananiev, R., Cherniykh, D., Khortov, A., Semiletov, I., Mayer, L. & Jerram, K., 2016, Evidence for an ice shelf covering the central Arctic Ocean during the penultimate glaciation: Nature Communications, v. 7, p. 1 – 10.

Klaebe, R. M., Smith, M. P., Fairchild, I. J., Fleming, E. J. & Kennedy, M. J., 2017, Facies-dependent $\delta^{13}C$ variation and diagenetic overprinting at the onset of the Sturtian glaciation in North-East Greenland: Precambrian Research (available online 13 December 2017), p. 1 – 18.

Kleine, B. I., Zhao, Z. & Skelton, A. D. L., 2016, Rapid fluid flow among fractures at greenschist facies conditions on Syros, Greece: American Journal of Science, v. 316, p. 169 – 201.

Lambeck, K., Rouby, H., Purcell, A., Sun, Y. & Sambridge, M., 2014, Sea level and global ice volumes from the Last Glacial Maximum to the Holocene: PNAS, v. 111, no. 43, p. 15296 – 15303.

Le Heron, D. P., Cox, G., Trundley, A. & Collins, A. S., 2011, Two Cryogenian glacial successions compared: Aspects of the Sturt and Elatina sediment records of South Australia: Precambrian Research, v. 186, p. 147 – 168.

Li, Z. X., Bogdanova, S. V., Collins, A. S., Davidson, A., de Waele, B., Ernst, R. E., Fitzsimons, I. C. W., Fuck, R. A., Gladkochub, D. P., Jacobs, J., Karlstrom, K. E., Lu, S., Natapov, L. M., Pease, V., Pisarevsky, S. A., Thrane, K. & Vernikovsky, V., 2008, Assembly, configuration, and break-up history of Rodinia: a synthesis: Precambrian Research, v. 160, p. 179 – 210.

Li, Z.-X., Evans, D. A. D. & Halverson, G. P., 2013, Neoproterozoic glaciations in a revised global palaeogeography from the breakup of Rodinia to the assembly of Gondwanaland: Sedimentary Geology, v. 294, p. 219 – 232.

Lisiecki, L. E. & Raymo, M. E., 2005, A Pliocene-Pleistocene stack of 57 globally distributed benthic $\delta^{18}O$ records: Paleoceanography, v. 20, p. 1 – 17.

Löwemark, L., Jakobsson, M., Mörth, M. & Backman, J., 2008, Arctic Ocean manganese contents and sediment colour cycles: Polar Research, v. 27, p. 105 – 113.

Naish, T. R., Woolfe, K. J., Barret, P. J., Wilson, G. S., Atkins, C., Bohaty, S. M., Bucker, C. J., Claps, M., Davey, F. J., Dunbar, G. B., Dunn, A. G., Fielding, C. R., Florindo, F., Hannah, M. J., Harwood, D. M., Henrys, S. A., Krissek, L. A., Lavelle, M., van der Meer, J., McIntosh, W. C., Niessen, F., Passchler, S., Powell, R. D., Roberts, A. P., Sagnotti, L., Scherer, R. P., Strong, C. P., Talarico, F., Verosub, K. L., Villa, G., Watkins, D. K., Webb, P-N. & Wonik, T., 2001, Orbitally induced oscillations in the East Antarctic ice sheet at the Oligocene/Miocene boundary: Nature, V. 413, P. 719 – 723.

Nesbitt, H. W. & Young, G. M., 1982, Early Proterozoic climates and plate motions inferred from major element chemistry of lutites: Nature, v. 299, p. 715 – 717.

Nilsson, J., Jakobsson, M., Borstad, C., Kirchner, N., Björk, G., Pierrehumbert, R. T. & Stranne, C., 2017, Ice-shelf damming in the glacial Arctic Ocean: dynamical regimes of a basin-covering kilometer-thick ice shelf: The Cryosphere, v. 11, p. 1745 – 1765.

Olympus Innov-X Delta User Manual, PN_103201, Rev_A: June/2010.

O'Regan, M., King, J., Backman, J., Jakobsson, M., Päilike, H., Moran, K., Heil, C., Sakamoto, T., Cronin, T. M. & Jordan, R. W., 2008: Constraints on the Pleistocene chronology of sediments from the Lomonosov Ridge: Paleoceanography, v. 23, p. 1 – 18.

Paillard, D., 2015, Quaternary glaciations: from observations to theories: Quaternary Science Reviews, v. 107, p. 11 – 24.

Prave, A. R., Fallick, A. E., Thomas, C. W. & Graham, C. M., 2009, A composite C-isotope profile for the Neoproterozoic Dalradian Supergroup of Scotland and Ireland: Journal of the Geological Society, v. 166, p. 845 – 857.

Rooney, A. D., Strauss, J. V., Brandon, A. D. & Macdonald, F. A., 2015, A Cryogenian chronology: Two long lasting synchronous Neoproterozoic glaciations: Geology, v. 43, p. 459 – 462.

Ruddiman, W. F., 2014, Earth's Climate – Past and Future (third edition): New York, W. H. Freeman and Company, 445 p.

Sellén, E., Jakobsson, M. & Backman, J., 2007, Sedimentary regimes in Arctic's Amerasian and Eurasian Basins: Clues to differences in sedimentation rates: Global and Planetary Change, v. 61., p. 275 – 284.

Sellén, E., O'Regan, M. & Jakobsson, M., 2010, Spatial and temporal Arctic Ocean depositional regimes: a key to the evolution of ice drift and current patterns: Quaternary Science Reviews, v. 29, p. 3644 – 3664.

Skelton, A. D. L., Graham, C. M. & Bickle, M. J., 1995, Lithological and structural controls on regional 3-D fluid flow patterns during greenschist facies metamorphism of the Dalradian of the SW Scottish Highland: Journal of Petrology, v. 36, p. 563- 586.

Skelton, A., Lewerentz, A., Kleine, B., Webster, D. & Pitcairn, I., 2015, Structural channeling of Metamorphic fluids on Islay, Scotland: Implications for Paleoclimatic reconstruction: Journal of Petrology, v. 56, p. 2145 – 2171.

Tziperman, E., Itay-Halevy, Johnston, D. T., Knoll, A. H. & Schrag, D. P., 2011, Biologically induced initiation of Neoproterozoic Snowball-Earth events, v. 108, p. 15091 – 15096.

Webster, D., Anderton, R. & Skelton, A., 2017, A guide to the geology of Islay (second edition): Ringwood Publishing, Glasgow, 178 p.

Wilson, G. S., Levy, R. H., Naish, T. R., Powell, R. D., Florindo, F., Ohneiser, C., Sagnotti, L., Winter, D. M., Cody., R., Henrys, S., Ross, J., Krissek, L., Niessen, F., Pampillio, M., Scherer, R., Alloway, B. V., Barret, P. J., Brachfeld, S., Browne, G., Carter, L., Cowan, E., Crampton, J., DeConto, R. M., Dunbar, G., Dunbar, N., Dunbar, R., von Eynatten, H., Gebhardt, C., Giorgetti, G., Graham, I., Hannah, M., Hansaraj, D., Harwood, D. M., Hinnov, L., Jarrad, R. D., Joseph, L., Kominz, M., Kuhn, G., Kyle, P., Läufer, A., McIntosh, W. C., McKay, R., Maffioli, P., Magens, D., Millan, C., Monien, D., Morin, R., Paulsen, T., Persico, D., Pollard, D., Raine, J. I., Riesselman, C., Sandroni, S., Schmitt, D., Sjunneskog, C., Strong, C. P., Talarico, F., Taviani, M., Villa, G., Vogel, S., Wilch, T., Williams, T., Wilson, T. J. & Wise, S., 2012, Neogene tectonic and climatic evolution of the Western Ross Sea, Antarctica – Chronology of events from the AND-1B drill hole: Global and Planetary Change, v. 96-97, p. 189 – 203.

Zachos, J., Pagani, M., Sloan, L., Thomas, E. & Billups, K., 2001, Trends, rhythms, and aberrations in global climate 65 Ma to present: Science, v. 292, p. 686 – 693.